2017

The P2X7 receptor antagonist Brilliant Blue G reduces serum human interferon-γ in a humanized mouse model of graft-versus-host disease

Nicholas Geraghty
University of Wollongong, ng646@uowmail.edu.au

Lisa Belfiore
University of Wollongong, lb989@uowmail.edu.au

Diane T. Ly
University of Wollongong, dly@uow.edu.au

Sam Adhikary
University of Wollongong, sra758@uowmail.edu.au

Stephen J. Fuller
University of Sydney

See next page for additional authors

Publication Details

Geraghty, N. J., Belfiore, L., Ly, D., Adhikary, S. R., Fuller, S. J., Varikatt, W., Sanderson-Smith, M. L., Sluyter, V., Alexander, S. I., Sluyter, R. & Watson, D. (2017). The P2X7 receptor antagonist Brilliant Blue G reduces serum human interferon-γ in a humanized mouse model of graft-versus-host disease. Clinical and Experimental Immunology, 190 (1), 79-95.

The P2X7 receptor antagonist Brilliant Blue G reduces serum human interferon-γ in a humanized mouse model of graft-versus-host disease

Abstract
Graft-*versus*-host disease (GVHD) remains a major problem after allogeneic haematopoietic stem cell transplantation, a curative therapy for haematological malignancies. Previous studies have demonstrated a role for the adenosine triphosphate (ATP)-gated P2X7 receptor channel in allogeneic mouse models of GVHD. In this study, injection of human peripheral blood mononuclear cells (PBMCs) into immunodeficient non-obese diabetic-severe combined immunodeficiency-interleukin (NOD-SCID-IL)-2Rγ^{null} (NSG) mice established a humanized mouse model of GVHD. This model was used to study the effect of P2X7 blockade in this disease. From five weeks post-PBMC injection, humanized mice exhibited clinical signs and histopathology characteristic of GVHD. The P2X7 antagonist, Brilliant Blue G (BBG), blocked ATP-induced cation uptake into both murine and human cells *in vitro*. Injection of BBG (50 mg/kg) into NSG mice did not affect engraftment of human leucocytes (predominantly T cells), or the clinical score and survival of mice. In contrast, BBG injection reduced circulating human interferon (IFN)-γ significantly, which was produced by human $CD4^+$ and $CD8^+$ T cells. BBG also reduced human T cell infiltration and apoptosis in target organs of GVHD. In conclusion, the P2X7 antagonist BBG reduced circulating IFN-γ in a humanized mouse model of GVHD supporting a potential role for P2X7 to alter the pathology of this disease in humans.

Disciplines
Medicine and Health Sciences

Publication Details
Geraghty, N. J., Belfiore, L., Ly, D., Adhikary, S. R., Fuller, S. J., Varikatt, W., Sanderson-Smith, M. L., Sluyter, V., Alexander, S. I., Sluyter, R. & Watson, D. (2017). The P2X7 receptor antagonist Brilliant Blue G reduces serum human interferon-γ in a humanized mouse model of graft-versus-host disease. Clinical and Experimental Immunology, 190 (1), 79-95.

Authors
Nicholas Geraghty, Lisa Belfiore, Diane T. Ly, Sam Adhikary, Stephen J. Fuller, W Varikatt, Martina L. Sanderson-Smith, Vanessa Sluyter, Stephen I. Alexander, Ronald Sluyter, and Debbie Watson

The P2X7 receptor antagonist Brilliant Blue G reduces serum human interferon-γ in a humanized mouse model of graft-versus-host disease

N.J. Geraghty[1,2,3], L. Belfiore[1,2,3], D. Ly[1,2,3], S.R. Adhikary[1,2,3], S.J. Fuller[4], W. Varikatt[5,6], M.L. Sanderson-Smith[1,2,3], V. Sluyter[1,2,3], S.I. Alexander[7], R. Sluyter[1,2,3] * and D. Watson[1,2,3] *

[1]School of Biological Sciences, University of Wollongong, Wollongong, NSW, 2252, Australia, [2]Centre for Medical and Molecular Biosciences, University of Wollongong, NSW, 2252, Australia, [3]Illawarra Health and Medical Research Institute, Wollongong, NSW, 2252, Australia, [4]Sydney Medical School Nepean, University of Sydney, Nepean Hospital, Penrith, NSW, 2750, Australia, [5]Sydney Medical School Westmead, University of Sydney, Westmead Hospital, Westmead, NSW, 2145, [6]Westmead Clinical School, University of Sydney, Pathology West, Institute for Clinical Pathology and Medical Research, Westmead Hospital, Westmead, NSW, 2145, Australia, [7]Children's Hospital at Westmead, Westmead, NSW, 2145, Australia

Correspondence to: R. Sluyter, Associate Professor, School of Biological Sciences, University of Wollongong, Illawarra Health and Medical Research Institute, Northfields Avenue, Wollongong, NSW 2522, Australia or D. Watson, Research Fellow, School of Biological Sciences, University of Wollongong, Illawarra Health and Medical Research Institute, Northfields Avenue, Wollongong, NSW 2522, Australia.

Email: rsluyter@uow.edu.au, dwatson@uow.edu.au

* R Sluyter and D Watson are co-senior authors.

KEY WORDS: Graft-versus-host disease, bone marrow transplantation, lymphocyte, P2X7 receptor, purinergic signalling, Brilliant Blue G, humanized mice

ABBREVIATIONS: Ab, antibody, APC, allophycocyanin, ATP, adenosine triphosphate, BBG, Brilliant Blue G, DC, dendritic cell, ELISA, enzyme-linked immunosorbent assay, FBS, heat-inactivated foetal bovine serum, FITC, fluorescein isothiocyanate, GVHD, graft-versus-host disease, h, human, HSCT, haematopoietic stem cell transplantation, i.p., intra-peritoneally, IFN, interferon, IL, interleukin, KO, knock-out, m, murine, mAb, monoclonal antibody, MST, median survival time, NSG, NOD-SCID-IL2Rγ^{null}, PBMC, peripheral blood mononuclear cell, PBS, phosphate buffered saline, PCR, polymerase chain reaction, PE, R-phycoerythrin, PerCP-Cy-5.5, peridinin chlorophyll protein, qPCR, quantitative real-time polymerase chain reaction, RT, room temperature, TBST, Tris-buffered saline containing 0.2% Tween-20, TBST2, Tris-buffered saline containing 0.05% Tween-20.

SUMMARY

Graft-versus-host disease (GVHD) remains a major problem after allogeneic haematopoietic stem cell transplantation, a curative therapy for haematological malignancies. Previous studies have demonstrated a role for the adenosine triphosphate (ATP)-gated P2X7 receptor channel in allogeneic mouse models of GVHD. In this study, injection of human peripheral blood mononuclear cells (PBMCs) into immunodeficient NOD-SCID-IL2Rγ^{null} (NSG) mice established a humanized mouse model of GVHD. This model was used to study the effect of P2X7 blockade in this disease. From five weeks post-PBMC injection, humanized mice exhibited clinical signs and histopathology characteristic of GVHD. The P2X7 antagonist, Brilliant Blue G (BBG), blocked ATP-induced cation uptake into both murine and human cells *in vitro*. Injection of BBG (50 mg/kg) into NSG mice did not affect engraftment of human leukocytes (predominantly T cells), or the clinical score and survival of mice. In contrast, BBG injection significantly reduced circulating human interferon (IFN)-γ, which was produced by human $CD4^+$ and $CD8^+$ T cells. BBG also reduced human T cell infiltration and apoptosis in target organs of GVHD. In conclusion, the P2X7 antagonist BBG reduced circulating IFN-γ in a humanized mouse model of GVHD supporting a potential role for P2X7 to alter the pathology of this disease in humans.

INTRODUCTION

Allogeneic haematopoietic stem cell transplantation (HSCT) is a current curative therapy for a range of haematological malignancies, including leukaemia and lymphoma [1]. A common complication following transplantation is the development of graft-versus-host disease (GVHD), which arises in approximately half of HSCT recipients worldwide [2]. GVHD is mediated by transplanted donor immune cells attacking "foreign" host tissue, resulting in inflammatory damage to healthy host tissue. The initial host tissue damage by pre-conditioning regimes used to treat cancer causes a pro-inflammatory environment, which in turn leads to activation of donor $CD4^+$ T cells through host antigen presenting cells [3]. $CD4^+$ T cells then release additional pro-inflammatory cytokines including interferon (IFN)-γ and interleukin (IL)-17, directly causing damage to tissue, as well as activating cytotoxic $CD8^+$ T cells which further exacerbate disease [4,5]. Current therapies aim to prevent GVHD by preventing these T cell responses through general immunosuppression, leaving a patient vulnerable to subsequent infection or relapse, demonstrating a vital need for novel therapeutics [6].

The purinergic system comprises a complex network of extracellular signalling molecules and plasma membrane receptors, and is involved in a range of physiological processes including inflammation and immunity [7]. Adenosine triphosphate (ATP) is a common signalling molecule in this system, acting as both an autocrine activation molecule, and a danger associated molecular pattern when released by damaged or dying cells [8]. In these contexts, extracellular ATP predominantly mediates its effects through activation of the P2X7 receptor [8]. P2X7 is an ATP-gated cation channel, whereby activation by ATP allows the flux of Ca^{2+}, K^+ and other cations including fluorescent dyes [9]. P2X7 is present on numerous immune cell types including antigen presenting cells and T cells [10]. Activation of

the P2X7 receptor can result in a variety of downstream signalling events including cytokine release, reactive oxygen species formation and cell proliferation [11].

Extracellular ATP and P2X7 have emerging roles in GVHD. In allogeneic mouse models, extracellular ATP accumulates at sites of inflammatory damage, whilst P2X7 is upregulated on dendritic cells (DCs) in lymphoid tissues and livers of mice with severe GVHD [12]. Notably, pharmacological blockade or genetic deletion of P2X7 reduces disease severity and improves survival in allogeneic mouse models of GVHD [12-14]. Studies investigating the role of P2X7 in human GVHD are limited, but it has been shown that P2X7 expression is higher in colon biopsies from HSCT patients [12]. Additionally, the presence of a loss-of-function *P2RX7* single nucleotide polymorphism (E496A) in either the donor or recipient cells correlates to reduced survival after allogeneic HSCT [15].

Therefore, the current study aimed to investigate the effect of the P2X7 antagonist, Brilliant Blue G (BBG), in a pre-clinical humanized mouse model of GVHD. BBG prevented ATP-induced dye uptake into splenic DCs from NOD-SCID-IL2Rγ^{null} (NSG) mice and peripheral blood T cells from humans. NSG mice engrafted with human (h) peripheral blood mononuclear cells (PBMCs) demonstrated increased P2X7 expression in the spleen and small intestine. Injection of BBG did not alter the engraftment of human leukocytes or the clinical signs of GVHD in these mice. In contrast, injection of BBG caused a significant reduction in serum hIFN-γ concentrations, and reduced human T cell infiltration and apoptosis in target organs, suggesting a potential role for P2X7 in GVHD pathogenesis in humans.

METHODS

Antibodies for flow cytometry

Fluorescein isothiocyanate (FITC) conjugated mouse anti-hCD4 (clone: RPA-T4), mouse anti-hCD8 (clone: RPA-T8) and mouse anti-hCD45 (clone: HI30) monoclonal antibodies (mAb); R-phycoerythrin (PE) conjugated mouse anti-hCD3 (clone: UCHT1) and mouse anti-hCD8 (clone: RPA-T8) mAb; peridinin chlorophyll protein (PerCP-Cy5.5) conjugated mouse anti-hCD4 (clone: L200) and rat anti-mCD45 (clone: 30-F11) mAb; allophycocyanin (APC) conjugated mouse anti-hCD3 (clone: UCHT1) and mouse anti-hCD19 (clone: HIB19) mAb were obtained from BD Pharmingen (San Jose, CA, USA). PE-conjugated hamster anti-murine (m) CD11c mAb (clone: N418) was from BioLegend (San Diego, CA, USA).

Cells

Human multiple myeloma RPMI8226 cells were obtained from the European Collection of Cell Cultures (Wiltshire, UK). Murine macrophage RAW264.7 cells were obtained from the American Type Culture Collection (Manassas, VA, USA). Cells were maintained in RPMI 1640 medium containing 2 mM GlutaMAX (Thermo Fisher Scientific, Waltham, MA, USA) and 10% heat-inactivated foetal bovine serum (FBS) (Bovogen Biologicals; East Keller, Australia) at 37°C/5% CO_2. Cell lines were checked every two months for *Mycoplasma spp.* infections, using a MycoAlert^{TM} Mycoplasma detection Kit (Lonza; Basel, Switzerland) as per the manufacturer's instructions. Cells were routinely negative for *Mycoplasma spp.*

Mice

Mouse experiments were approved by the Animal Ethics Committee, University of Wollongong (Wollongong, Australia). C57BL/6 mice were obtained from Australian BioResources (Moss Vale, Australia). P2X7 knock-out (KO) mice [16], backcrossed onto a C57BL/6 background [17] were bred at the University of Wollongong. Deletion of the

P2RX7 gene was periodically confirmed as described [16]. Female NSG mice, originally obtained from The Jackson Laboratory (Bar Harbor, ME, USA), were bred at the Westmead Animal Research Facility (Westmead, Australia). NSG mice were housed in filter top cages in Tecniplast (Buggugiate, Italy) isolation cabinets, and provided with autoclaved food and water, *ad libitum*.

Isolation of human PBMCs

Experiments with human blood were approved by the Human Ethics Committee, University of Wollongong. Blood was collected by venepuncture into VACUETTE® lithium heparin tubes (Greiner Bio-One; Frickenhausen, Germany). Whole blood was diluted with an equal volume of sterile phosphate buffered saline (PBS) (Thermo Fisher Scientific), underlaid with Ficoll-Paque PLUS (GE Healthcare; Uppsala, Sweden) and centrifuged (560 x g for 30 min). hPBMCs were collected and washed with two volumes of PBS by centrifugation (430 x g for 5 min) and resuspended in PBS.

Humanized mouse model of GVHD

NSG mice were injected intra-peritoneally (i.p) with 10 x 10^6 hPBMCs in 100 µL sterile PBS (hPBMC group), or with 100 µL sterile PBS alone (control group) (day 0). At 3 weeks post-hPBMC injection, mice were checked for engraftment by immunophenotyping of tail vein blood. Mice were monitored up to week 8 or 10 for signs of GVHD using a scoring system (involving a score out of 2, for each of the following five criteria; weight loss, hunching, decreased activity, fur ruffling, and skin involvement) giving a total clinical score out of 10. Mice were euthanized at 8 or 10 weeks post-injection of hPBMCs, or earlier if exhibiting a clinical score of ≥ 8 or a weight loss of ≥ 10%, according to the approved animal ethics protocol. For BBG blockade, mice were injected with 10 x 10^6 hPBMCs as above, and with either 200 µL sterile saline (saline group), or 200 µL sterile saline containing BBG (50

mg/kg) (BBG group) (Sigma-Aldrich; St Louis, MO, USA) on days 0 (1 h post-hPBMC injection), 2, 4, 6 and 8.

Immunophenotyping by flow cytometry

Tail vein blood (50 μL) was collected into 200 μL of citrate solution (Sigma-Aldrich), diluted with PBS and centrifuged (500 x g for 5 min). Spleens from euthanized mice were homogenized and filtered through 70 μm nylon filters (Falcon Biosciences, New York, NY, USA) and centrifuged (300 x g for 5 min). Blood and spleen cells were incubated with ammonium chloride potassium lysis buffer (150 mM NH_4Cl, 1 mM $KHCO_3$, 0.1 mM Na_2CO_3, pH 7.3) for 5 min and washed in PBS (300 x g for 5 min). Cells were washed in PBS containing 2% FBS (300 x g for 3 min), and incubated for 30 min with fluorochrome conjugated mAb, including respective isotype controls. Cells were washed with PBS (300 x g for 3 min) and data was collected using a BD Biosciences LSRII Flow Cytometer (using band pass filters 515/20 for FITC, 575/26 for PE, 675/40 for PerCP-Cy5.5, and 660/20 for APC). The relative percentages of cells were analyzed using FlowJo software v8.7.1 (TreeStar Inc.; Ashland, OR, USA) (Fig. S1 and Fig. S2).

Histological analysis

Tissues from euthanized mice were incubated overnight in neutral buffered (10%) formalin (Sigma-Aldrich). Fixed tissues were removed, coated in paraffin, sectioned (5 μm) and stained with haematoxylin and eosin (POCD; Artarmon, Australia). Histological changes were assessed using a Leica (Wetzlar, Germany) DMIL inverted light microscope at 4x objective and images captured using a Motic (Causeway Bay, Hong Kong) Moticam 2 microscope camera, and using Motic Images Plus software v2.0.

Isolation of RNA

Tissues removed from euthanized mice were stored in RNAlater (Sigma-Aldrich) at -20°C until required. RNA was isolated using TRIzol reagent (Thermo Fisher Scientific) as per the manufacturer's instructions. Isolated RNA was immediately converted to complementary DNA (cDNA), using the qScript cDNA Synthesis Kit (Quanta Biosciences, Beverly, MA, USA) as per the manufacturer's instructions, and stored at -80°C. cDNA was checked by PCR amplification of the house keeping gene glyceraldehyde 3-phosphate dehydrogenase (Invitrogen, Carlsbad, CA, USA) for 35 cycles (95°C for 1 min, 55°C for 1 min, and 72°C for 1 min) and a holding temperature of 4°C. Purity and size of amplicons were confirmed by 2% agarose gel electrophoresis.

Quantitative real-time PCR

Quantitative real-time PCR (qPCR) reactions were performed using TaqMan Universal Master Mix II (Thermo Fisher Scientific) according to the manufacturer's instructions, with primers for FAM-labelled murine glyceraldehyde 3-phosphate dehydrogenase (Mm99999915_g1) and mIL-1β (Mm00434228_m1), and VIC-labelled mP2X7 (Mm01199503_m1), and primers for FAM-labelled human hypoxanthine phosphoribosyl transferase 1 (Hs99999909_m1) and hIL-1β (Hs01555410_m1), and VIC-labelled hIFN-γ (Hs00989291_m1), hIL-17 (Hs00936345_m1), and hP2X7(B) (AIOIXC2) (Thermo Fisher Scientific), as indicated. qPCR cycles consisted of two initial steps of 50°C for 2 min, and 95°C for 10 min and 40 cycles of 95°C for 15 s, and 60°C for 1 min. qPCR reactions were conducted in triplicate, and were performed on a Roche Diagnostics (Indianapolis, IN, USA) LightCycler 480, and analysis was conducted using LightCycler480 software v1.5.1.

Immunoblotting

Cell lysates were prepared and immunoblotting was performed as described [18]. Briefly, cell lysates (15 μg protein per lane) were loaded into a Mini-PROTEAN TGXTM Precast Gel (Bio-Rad, Hercules, CA, USA) and electrophoresed. Proteins were transferred to a nitrocellulose membrane (Bio-Rad) using a Bio-Rad Trans-Blot Turbo Blotting System. Membranes were washed with Tris-buffered saline (250 mM NaCl and 50 mM Tris, pH 7.5) containing 0.2% Tween-20 (TBST) and blocked overnight at 4°C with blocking solution (TBST containing 5% milk powder). Membranes were incubated with rabbit anti-mP2X7 (extracellular epitope) antibody (Ab) (1:500) (Alomone Labs; Jerusalem, Israel) for 2 h at room temperature (RT), washed with TBST and incubated with peroxidase-conjugated goat anti-rabbit immunoglobulin G (1:1000) (Rockland Immunochemicals; Limerick, PA, USA) for 1 h at RT. Membranes were washed with TBST and incubated with SuperSignal West Pico Chemiluminescent Substrate (Thermo Fisher Scientific) and images collected using an Amersham Imager600 (GE Healthcare).

ATP-induced YO-PRO-1^{2+} uptake assay

P2X7 pore formation was quantified by measuring ATP-induced YO-PRO-1^{2+} uptake as previously described [19]. Briefly, cells in NaCl medium (145 mM NaCl, 5 mM KCl, 5 mM glucose and 10 mM HEPES, pH 7.4) at 37°C were incubated in the absence or presence of BBG for 15 min, and then incubated with 1 μM YO-PRO-1 iodide (Molecular Probes, Eugene, OR, USA) in the absence or presence of 1 mM ATP (Sigma-Aldrich) for 10 min. Incubations were stopped by addition of ice-cold NaCl medium containing 20 mM $MgCl_2$ ($MgCl_2$ medium) and centrifugation (300 x g for 3 min). Cells were incubated with PE-conjugated anti-mCD11c or APC-conjugated anti-hCD3 mAb, respectively where indicated, for 15 min and washed with NaCl medium. Data was collected using an LSRII Flow Cytometer (band-pass filter 515/20 for YO-PRO-1^{2+}, 575/25 for PE and 660/20 for APC) and

FACSDiva software version 8.0. Geometric mean fluorescence intensity of YO-PRO-1^{2+} uptake was analyzed using FlowJo software (Fig. S3).

Immunohistochemistry

Paraffin-embedded formalin fixed tissues were sectioned (5 μm) and mounted on Snowcoat slides (Leica) coated with porcine gelatin (Sigma-Aldrich). To identify T cells, tissue sections were deparaffinised and heat induced epitope retrieval was performed by incubating in sodium citrate buffer (10 mM trisodium citrate dehydrate (Sigma-Aldrich) and 0.05% Tween-20) for 20 min at 95°C. Before all subsequent steps, tissue sections were washed with Tris-buffered saline (138 mM NaCl, 2.7 mM KCl and 50 mM Tris, pH 7.5) containing 0.05% Tween-20 (TBST2). Tissue sections were blocked with PBS containing 20% goat serum (Thermo Fisher Scientific) and 3% bovine serum albumin (BSA) (Amresco, Solon, OH, USA) for 30 min at RT, and subsequently incubated with rabbit anti-hCD3 mAb (clone: EP449E) (1:50) (Abcam, Cambridge, UK) in TBST2 containing 1% BSA overnight at 4°C. Endogenous peroxidase was quenched by incubating with 3% hydrogen peroxide in PBS containing 1% BSA for 20 min at RT. Tissue sections were then incubated with horseradish peroxidase-conjugated goat anti-rabbit immunoglobulin G (1:250) (Invitrogen) in TBST containing 1% BSA for 15 min at RT. Finally, tissue sections were incubated with 3,3 diaminobenzidine tetrachloride (Sigma-Aldrich) for 5 min at RT, counterstained with haematoxylin and dehydrated. To identify apoptotic cells, an *In situ* Apoptosis Detection Kit (Abcam) was used as per the manufacturer's instructions. Immunohistochemistry images were captured using a Leica DMRB microscope and Leica Application Software version 4.3.

ELISA

Blood, collected via cardiac puncture from euthanized mice, was incubated for 1 h at RT and centrifuged (1,700 x g for 10 min). Supernatants were re-centrifuged (1,700 x g for 10 min)

and sera stored at -80°C. Serum cytokine concentrations were measured using hIFN-γ, hIL-17, hIL-4 and mIL-1β Ready-Set-Go! ELISPOT Kits (eBioscience, San Diego, CA, USA) as per the manufacturer's instructions. Absorbance (450 and 570 nm) was measured using a SpectraMax Plus 384 (Molecular Devices, Sunnyvale, CA, USA).

Intracellular staining

Splenocytes, following ammonium chloride potassium buffer lysis, were incubated for 4 h in RPMI 1640 medium containing 2 mM L-glutamine (Thermo Fisher Scientific), 10% FBS, 1% non-essential amino acids (Thermo Fisher Scientific), 55 μM mercaptoethanol (Thermo Fisher Scientific), 100 U/mL penicillin/100 μg/mL streptomycin (Thermo Fisher Scientific), 50 ng/mL phorbol 12-myristate 13-acetate (Sigma-Aldrich), 1 μg/mL ionomycin (Sigma-Aldrich), and 1 μg/mL GolgiStop^{TM} (BD Biosciences). Cells were centrifuged (300 x g for 5 min) and washed once with PBS (300 x g for 5 min). Staining was performed using the BD Biosciences Intracellular Stain Kit as per the manufacturer's instructions, mAb added and incubated for 30 min at RT. Cells were washed with PBS and data was collected using an LSRII Flow Cytometer (band-pass filter 515/20 for FITC, 575/25 for PE, 675/40 for PerCP-Cy5.5 and 660/20 for APC) and FACSDiva software version 8.0. The percentage of hIFN-γ^+ and hIL-17^+ cells was analyzed using FlowJo software (Fig. S4).

Statistical Analysis

Data is given as mean ± standard error of the mean (SEM). Statistical differences were calculated using Student's t-test for single comparisons or one-way analysis of variance (ANOVA) with Tukey's post-hoc test for multiple comparisons. Weight and clinical score were analyzed using a repeated measures two-way ANOVA. Survival was compared using the log-rank (Mantel-Cox) test. Correlations between cytokines were assessed using Spearman correlation. All statistical analyses and graphs were generated using GraphPad

Prism 5 for PC (GraphPad Software, La Jolla, CA, USA). $P < 0.05$ was considered significant for all tests.

RESULTS

NSG mice injected with hPBMCs engraft predominantly human CD3$^+$ T cells and exhibit clinical signs of GVHD

NSG mice injected with hPBMCs develop GVHD from 4 weeks [20]. In the current study, NSG mice were injected i.p. with 10 x 10^6 freshly isolated hPBMCs (hPBMC group) or saline (control group), and observed for signs of GVHD development for up to 8 weeks. At 3 weeks post-hPBMC injection, mice were checked for engraftment of human cells. hPBMC-injected mice demonstrated engraftment of human leukocytes (14.4 ± 2.7% hCD45$^+$ mCD45$^-$ cells, n = 9), whilst as expected, no human leukocytes were observed in three randomly selected control mice (Fig. 1a). In hPBMC-injected mice the majority of hCD45$^+$ cells were T cells (97.5 ± 0.3% hCD3$^+$ hCD19$^-$ cells, n = 9) (Fig. 1b). NSG mice injected with hPBMCs demonstrated no human B cell (hCD3$^-$ hCD19$^+$) engraftment (data not shown), and the remaining human leukocytes were negative for both hCD3 and hCD19 (2.5 ± 0.3%, n = 9) (Fig. 1c).

Analysis of spleens from mice euthanized at end point confirmed the absence of human leukocytes in control mice (n = 9) (Fig. 1d). hPBMC-injected mice engrafted large amounts of human leukocytes (86.4 ± 2.0% hCD45$^+$ mCD45$^-$ cells, n = 9), whilst as expected, no human leukocytes were observed in control mice (n = 9) (Fig. 1d). The majority of human leukocytes in the spleen were T cells (98.3 ± 0.2% hCD3$^+$ hCD19$^-$ cells, n = 9) (Fig. 1e). No human B cells (hCD3$^-$ hCD19$^+$) were found in the spleen (data not shown), and the remaining cells were negative for both hCD3 and hCD19 (1.7 ± 0.3%, n = 9) (Fig. 1f). Analysis of human T cells (hCD3$^+$) revealed that hPBMC-injected mice demonstrated a significantly higher percentage of hCD4$^+$ T cells (69.6 ± 6.6%, n = 9) compared to hCD8$^+$ T cells (27.6 ± 6.4%, n = 9) (P = 0.0121) (Fig. 1g).

As stated above, mice were observed for signs of GVHD for up to 8 weeks. Weight changes were similar between hPBMC-injected and control mice from weeks 1-4, with both groups demonstrating weight gain. However, hPBMC-injected mice steadily began to lose weight from day 30, while saline-injected control mice maintained a weight of over 110% of their starting weight throughout the 8 week observation period (P = 0.4154) (Fig. 1h). Saline-injected control mice did not show any signs of GVHD, and maintained a clinical score of 0 over the observation period (n = 9). In contrast, hPBMC-injected mice displayed clinical signs of GVHD from day 30, first evident as fur ruffling, followed by hunching, reduced activity, weight loss, and/or areas of scaly skin patches. hPBMC-injected mice had a mean clinical score of 4.3 ± 1.1 at end point. The clinical scores between the two groups were significantly different over 8 weeks (n = 9) (P = 0.0038) (Fig. 1i). hPBMC-injected mice succumbed to disease from day 40, with a median survival time (MST) of 54 days, and exhibited a 55% mortality rate by end point, compared to 100% survival of control mice (P = 0.0101) (Fig. 1j).

NSG mice injected with hPBMCs show histological evidence of GVHD and increased murine P2X7 expression

Histological analysis of the target organs; liver, small intestine and skin, revealed that mice injected with hPBMCs displayed greater leukocyte infiltration and tissue damage compared to tissues from control mice (Fig. 2a). Compared to control mice, hPBMC-injected mice demonstrated mildly increased leukocyte infiltration, loss of structural integrity and apoptosis of cells in the liver (Fig. 2a), mild damage in the small intestine with increased apoptotic cells and rounded villi (Fig. 2a), and lastly mild leukocyte infiltration and epidermal thickening in the skin compared to control mice (Fig. 2a).

P2X7 expression is up-regulated in host tissues in allogeneic mouse models of GVHD [12,14]. Therefore, mP2X7 expression in the spleen, liver and small intestine was analyzed by qPCR. mP2X7 expression was increased two-fold in the spleens from hPBMC-injected mice (2.6 ± 0.6, n = 7) compared to spleens from control mice (1.2 ± 0.6, n = 4), but this difference did not reach statistical significance (P = 0.1656) (Fig. 2b). Hepatic mP2X7 expression was similar in hPBMC-injected (5.5 ± 0.6, n = 6) and control mice (6.9 ± 1.4, n = 3) (P = 0.4160) (Fig. 2c). mP2X7 expression was approximately two-fold greater in the small intestines from hPBMC-injected mice (16.9 ± 2.7, n = 6) compared to control mice (9.9 ± 6.2, n = 4), but this did not reach statistical significance (P = 0.2668) (Fig. 2d).

NSG mice express full-length functional P2X7 receptors

The data above (Fig. 2b-d) demonstrates that NSG mice express P2X7, but it remained unknown if NSG mice express functional P2X7. Immunoblotting using an antibody against the extracellular domain of P2X7 demonstrated a major band at 81 kDa, corresponding to full-length P2X7 [21] in the positive control RAW264.7 macrophages and in NSG splenocytes (n = 2) (Fig. 3a).

To determine if NSG mice express functional P2X7, RAW264.7 cells or splenic leukocytes from mice were incubated in the absence or presence of ATP, and YO-PRO-1^{2+} uptake assessed by flow cytometry. ATP induced YO-PRO-1^{2+} uptake into positive control RAW264.7 cells (n = 4) and $CD11c^+$ splenic DCs from C57BL/6 mice (n = 4), but not negative control $CD11c^+$ splenic DCs from P2X7 KO mice (n = 3) (Fig. 3b). Notably, ATP also induced YO-PRO-1^{2+} uptake into $CD11c^+$ splenic DCs from NSG mice (n = 5) (Fig 3b). This uptake was 50% lower than that of RAW264.7 macrophages (P < 0.005), but three-fold greater than that of C57BL/6 $CD11c^+$ splenic DCs (P < 0.005) (Fig. 3b).

BBG prevents ATP-induced cation uptake into human and murine leukocytes

Since its initial use in rodent models of multiple sclerosis [22], spinal cord injury [23] and Huntington's disease [24], BBG has been used in over 40 studies to establish the role of P2X7 in various disorders [25] including our group in a murine model of amyotrophic lateral sclerosis [26]. To confirm that BBG can block hP2X7 and mP2X7, human RPMI8226 and murine RAW264.7 cells, both of which express endogenous P2X7 [27,28], were pre-incubated with increasing concentrations of BBG and then ATP-induced YO-PRO-1^{2+} uptake was assessed. BBG exhibited a concentration-dependent inhibition of ATP-induced YO-PRO-1^{2+} uptake, with maximal inhibition at 1 μM in both cell types, and half maximal inhibitory concentrations (IC_{50}) of 99.0 ± 1.2 nM and 59.7 ± 1.2 nM in RPMI8226 cells and RAW264.7 cells, respectively (Fig. 4a). These IC_{50} values are similar to that known for recombinant hP2X7 and mP2X7 [25].

To confirm that BBG can block P2X7 in primary leukocytes, hPBMCs and NSG splenocytes were pre-incubated in the absence or presence of BBG, and then ATP-induced YO-PRO-1^{2+} uptake was assessed. ATP induced significant YO-PRO-1^{2+} uptake into $hCD3^+$ T cells, which was reduced by 95% by pre-incubation with BBG ($P < 0.0001$, $n = 3$) (Fig. 4b). ATP induced significant YO-PRO-1^{2+} uptake into NSG $CD11c^+$ splenic DCs, which was reduced 92% by pre-incubation with BBG (Fig. 4c) ($P < 0.0001$, $n = 3$). Basal uptake of YO-PRO-1^{2+} in the absence or presence of BBG was similar for each respective cell subtype (Fig. 4b, c).

BBG does not affect engraftment of human cells or prevent GVHD in NSG mice

To investigate whether P2X7 blockade can prevent disease in a humanized mouse model of GVHD, NSG mice were injected with hPBMCs and the P2X7 antagonist BBG (50 mg/kg)

was subsequently injected every two days from days 0 to 8. Mice were monitored for weight loss and signs of GVHD for up to 10 weeks. To determine if BBG affected engraftment of human cells, blood was collected at 3 weeks post-hPBMC injection and cells analyzed by flow cytometry. BBG-injected mice demonstrated a similar level of human leukocytes (10.4 ± 1.3% $hCD45^+$ $mCD45^-$ cells, n = 14) compared to saline-injected (vehicle control) mice (10.6 ± 1.4% $hCD45^+$ $mCD45^-$ cells, n = 16) (P = 0.9179) (Fig. 5a). In both groups of mice, the majority of $hCD45^+$ cells were T cells, which did not differ between BBG-injected mice (97.2 ± 0.4% $hCD3^+$ $hCD19^-$ cells, n = 14) and saline-injected mice (97.4 ± 0.4% $hCD3^+$ $hCD19^-$ cells, n = 16) (P = 0.7014) (Fig. 5b). Neither group of mice demonstrated engraftment of B cells ($hCD3^-$ $hCD19^+$) (data not shown). The remaining $hCD45^+$ cells were negative for both hCD3 and hCD19, and the percentage of these cells did not differ between BBG-injected mice (2.7 ± 0.4%, n = 14) and saline-injected mice (2.5 ± 0.4%, n = 16) (P = 0.8291) (Fig. 5c).

Analysis of spleens from all mice euthanized at end point demonstrated human leukocytes comprised the majority of total murine and human leukocytes. BBG-injected mice engrafted a similar level of human leukocytes (56.3 ± 5.0% $hCD45^+$ $mCD45^-$ cells, n = 13) compared to saline-injected mice (56.2 ± 6.2% $hCD45^+$ $mCD45^-$ cells, n = 15) (P = 0.9899) (Fig. 5d). The majority of human leukocytes in the spleen were T cells, and both BBG-injected mice (97.1 ± 0.6% $hCD3^+$ $hCD19^-$ cells, n = 13) and saline-injected mice (95.4 ± 0.6% $hCD3^+$ $hCD19^-$ cells, n = 15) demonstrated similar percentages of T cells (P = 0.2481) (Fig. 5e). No human B cells ($hCD3^-$ $hCD19^+$) were found in the spleens (data not shown). The remaining $hCD45^+$ cells were negative for both hCD3 and hCD19, and percentages of these cells did not differ between BBG-injected mice (2.7 ± 0.6%, n = 15) and saline-injected mice (2.7 ± 0.6%, n = 15) (P = 0.5325) (Fig. 5f). Analysis of the human T cells ($hCD3^+$) revealed that BBG- and saline-injected mice contained similar percentages of $hCD4^+$ T cells (67.0 ± 4.1%, n = 13

vs. 72.7 ± 4.3%, n = 15, respectively, P = 0.3515). BBG- and saline-injected mice also contained similar percentages of $hCD8^+$ T cells (24.0 ± 3.6%, n = 13 vs 22.3 ± 4.1%, n = 15, respectively, P = 0.7583). In both BBG- and saline-injected mice, the percentage of $hCD4^+$ T cells was significantly higher than $hCD8^+$ T cells (P < 0.0001) (Fig. 5g).

As stated above, mice were observed for signs of GVHD for up to 10 weeks. Both BBG- and saline-injected humanized mice began to lose weight from day 30 (P = 0.8450) (Fig. 5h). Both BBG- and saline-injected mice began to exhibit signs of mild GVHD at day 35, and both BBG- and saline-injected mice, exhibited similar clinical scores at end point (5.3 ± 0.5, n = 16 vs. 4.9 ± 0.6, n = 14, respectively). The clinical scores between the two groups were not significantly different over 8 weeks (P = 0.8356) (Fig. 5i). Survival was also similar in both BBG-injected mice (MST of 64 days, and mortality rate of 57%, n = 16) and saline-injected mice (MST of 60 days and mortality rate of 62%, n = 14), (P = 0.9874 for mortality rate) (Fig. 5j).

BBG reduces histological evidence of GVHD in humanized mice

BBG- and saline-injected humanized mice demonstrated similar damage to the liver with some leukocyte infiltration, apoptosis of cells and fibrosis (Fig. 6a). Both BBG- and saline-injected humanized mice demonstrated structural damage to the small intestine; however, BBG-injected humanized mice exhibited decreased leukocyte infiltration compared to saline-injected humanized mice (Fig. 6a). BBG-injected humanized mice also exhibited mildly decreased leukocyte infiltrates in the dermis, decreased apoptotic cells and reduced basal vacuolar change of the skin compared to that of saline-injected humanized mice (Fig. 6a).

Immunohistochemistry of the target organs, liver, small intestine and skin, was used to determine if the leukocyte infiltrates observed above included human T cells. T cells

(indicated by black arrows) were identified in the liver, and to a lesser extent in the small intestine and skin (Fig. 6b). T cell infiltration in the liver, small intestine and skin appeared to be reduced in BBG-injected mice compared to saline-injected mice (Fig. 6b). To confirm tissue damage in the liver, small intestine and skin, these target organs were analyzed for evidence of apoptosis (fragmented DNA) by immunohistochemistry. Apoptotic cells (indicated by red arrows) were evident in the liver and small intestine, and to a lesser extent in the skin (Fig. 6c). Apoptosis in these organs appeared to be reduced in BBG-injected mice compared to saline-injected mice (Fig. 6c).

BBG-injected mice demonstrate similar mP2X7 and hP2X7 expression in GVHD target organs

To determine whether injection of BBG altered expression of murine (host) or human (donor) P2X7 expression in the spleens and target organs of GVHD, tissues from humanized mice were analyzed by qPCR. mP2X7 expression was similar in spleens of BBG-injected mice (4.6 ± 1.0, $n = 6$) and saline-injected mice (5.7 ± 0.5, $n = 6$) ($P = 0.5446$) (Fig. 7a). mP2X7 expression in the liver was reduced by 58% in BBG-injected mice (1.6 ± 0.3, $n = 4$) compared to saline-injected mice (3.9 ± 1.2, $n = 5$), however this difference did not reach statistical significance ($P = 0.1619$) (Fig. 7b). Conversely, mP2X7 expression was increased almost two-fold in the small intestines of BBG-injected mice (2.8 ± 0.7, $n = 6$) compared to saline-injected mice (1.6 ± 0.3, $n = 5$), but this did not reach statistical significance ($P = 0.1763$) (Fig. 7c). hP2X7 expression was decreased by 74% in the spleens of BBG-injected mice (3.0 ± 0.9, $n = 5$) compared to saline-injected mice (11.4 ± 3.5, $n = 6$) and this difference approached statistical significance ($P = 0.0595$) (Fig. 7d). In contrast, hP2X7 expression was similar in the livers and small intestines of BBG-injected mice (6.3 ± 2.6, $n =$

5, and 7.6 ± 2.9, n = 5, respectively) compared to saline-injected mice (3.7 ± 1.1, n = 4, and 5.7 ± 1.8, n = 6, respectively) (P = 0.4296 and 0.5642, respectively) (Fig. 7e, 7f).

BBG reduces serum human IFN-γ in humanized mice

IFN-γ and IL-17 are important pro-inflammatory cytokines implicated in the pathogenesis of GVHD [4,5]. To determine if BBG treatment altered the amount of these cytokines, serum hIFN-γ and hIL-17 concentrations in humanized mice were assessed by ELISA. hIFN-γ was present in the serum of all mice for which samples were available (Fig. 8a). Notably, treatment with BBG significantly reduced the amount of serum hIFN-γ in BBG-injected mice (10.0 ± 2.4 ng/mL, n = 12), which was 54% lower than that of saline-injected mice (21.8 ± 2.4 ng/mL, n = 13) (P = 0.0023) (Fig. 8a). In contrast, hIL-17 was only detected in the serum from four BBG-injected mice (33%) and two saline-injected mice (15%) for which samples were available (Fig. 8b). The amount of hIL-17 in the serum of BBG-injected mice (40.8 ± 21.1 pg/mL, n = 4) was almost ten-fold greater than that of saline-injected mice (4.4 ± 4.0 pg/mL, n = 2), however this difference did not reach statistical significance (P = 0.1031) (Fig. 8b).

To determine the potential source of hIFN-γ and hIL-17, splenocytes were isolated from humanized mice and the intracellular expression of hIFN-γ and hIL-17 was analyzed by flow cytometry. Both $hCD4^+$ and $hCD8^+$ T cells produced hIFN-γ and to a lesser extent hIL-17 (Fig. 8c, 8d). The percentage of hIFN-γ-producing $hCD8^+$ T cells was four-fold greater than hIFN-γ-producing $hCD4^+$ T cells from BBG-injected mice (32.6 ± 7.1% vs 8.1 ± 2.1%, respectively, n = 4) and saline-injected mice (39.0 ± 18.9% vs 10.2 ± 7.3%, respectively, n = 3), but this only reached statistical significance in the BBG-injected group (P = 0.0165) (Fig. 8c). The percentage of hIL-17-producing $hCD4^+$ and $hCD8^+$ T cells in BBG-injected mice (3

± 4% vs. 2 ± 1%, $n = 4$, respectively) was similar to saline-injected mice (2 ± 1% vs. 2 ± 1%, $n = 3$, respectively) ($P = 0.5046$ and 0.8437, respectively) (Fig. 8d).

To determine if expression of IFN-γ and IL-17 were altered in the spleens, and target organs of GVHD, tissues from humanized mice were analyzed by qPCR. hIFN-γ expression was 1.5-fold greater in the spleens of BBG-injected mice (9.4 ± 3.9, $n = 6$) compared to saline-injected mice (6.4 ± 1.2, $n = 6$), but this difference did not reach statistical significance ($P = 0.4825$) (Fig 8e). hIFN-γ expression was similar in livers of BBG-injected mice (1.4 ± 0.1, $n = 6$) and saline-injected mice (1.6 ± 0.3, $n = 6$) ($P = 0.6549$) (Fig. 8f). hIFN-γ expression was two-fold greater in the small intestines of BBG-injected mice (2.5 ± 1.1, $n = 3$) compared to saline-injected mice (1.2 ± 0.1, $n = 4$) but again this difference did not reach statistical significance ($P = 0.2050$) (Fig. 8g). hIL-17 expression in spleens of BBG-injected mice (9.6 ± 6.3, $n = 5$) was similar to saline-injected mice (13.9 ± 4.0, $n = 6$) ($P = 0.5441$) (Fig. 8h). hIL-17 was not detected in the livers of either BBG-injected mice ($n = 2$) or saline-injected mice ($n = 4$) (Fig. 8i). hIL-17 expression was two-fold greater in the small intestines of BBG-injected mice (6.3 ± 2.2, $n = 5$) compared to saline-injected mice (2.6 ± 1.3, $n = 4$), but this difference did not reach statistical significance ($P = 0.2263$) (Fig. 8j).

BBG does not alter murine or human IL-1β expression in humanized mice

Activation of P2X7 causes IL-1β maturation and release from antigen presenting cells [29], a pro-inflammatory cytokine implicated in the pathogenesis of GVHD [30]. Moreover, P2X7-mediated IL-1β release is involved in the production of IFN-γ [31] and IL-17 [32]. Given the identity of the antigen presenting cells involved in human T cell activation in our humanized model of GVHD remains unknown and since mIL-1β can stimulate human cells [33,34], the expression of both mIL-1β and hIL-1β in the spleen, liver and small intestine from these mice was analyzed by qPCR. mIL-1β expression was 3-fold greater in the spleens of BBG-injected

mice (6.3 ± 2.8, n = 3) compared to saline-injected mice (2.0 ± 0.9, n = 5), but this difference did not reach statistical significance (P = 0.1183) (Fig. 9a). mIL-1β expression was similar in the livers and small intestines of BBG-injected (2.7 ± 1.2, n = 5 and 2.5 ± 0.5, n = 6, respectively) and saline-injected mice (2.7 ± 0.7, n = 4 and 1.9 ± 0.6, n = 6, respectively) (P = 0.9552 and 0.4829, respectively) (Fig. 9b, 9c). In contrast to mIL-1β, hIL-1β expression was approximately 50% lower in the spleens of BBG-injected mice (2.2 ± 1.1, n = 5) compared to saline-injected mice (5.0 ± 2.1, n = 5), but this difference did not reach statistical significance (P = 0.2986) (Fig. 9d). hIL-1β expression was not detected in livers or small intestines from either BBG- or saline-injected mice (both n = 5) (data not shown). Therefore, given the broad expression of mIL-1β within the humanized mice, mIL-1β in the serum of these mice was assessed by ELISA. However contrary to mIL-1β expression in tissues, mIL-1β was not detected in the serum from BBG-injected (0.0 ± 0.0, n = 12) or saline-injected mice (0.0 ± 0.0, n = 11) using an ELISA with a reported sensitivity of 8 pg/mL (eBioscience).

DISCUSSION

This study aimed to investigate the effect of the P2X7 antagonist, BBG, in a pre-clinical humanized mouse model of GVHD. Injection of BBG into humanized mice did not alter human leukocyte engraftment or disease progression, as assessed by weight loss, clinical score and survival. However, treatment with BBG significantly reduced serum hIFN-γ and reduced human splenic hIFN-γ mRNA expression. Intracellular hIFN-γ was detected in both splenic $hCD4^+$ and $hCD8^+$ T cells of humanized mice, with a larger proportion (four-fold) of hIFN-γ^+ $hCD8^+$ T cells than hIFN-γ $hCD4^+$ T cells. However, splenic $hCD4^+$ T cells were more frequent (three-fold) than $hCD8^+$ T cells in humanized mice, and therefore the relative contribution of each subset to circulating IFN-γ production needs to be further elucidated. Pharmacological blockade or genetic deficiency of P2X7 has also been shown to reduce serum IFN-γ in allogeneic mouse models of GVHD [12,13]. Additionally, P2X7 activation of the NLRP3 inflammasome and subsequent IL-1β production promotes the generation of IFN-γ^+ $CD8^+$ T cells in mice [31]. Combined, these findings support a potential role for P2X7 in GVHD pathology in humans, possibly through the regulation of T cell activation and subsequent IFN-γ production. To this end, IFN-γ plays important roles in the up-regulation of CXCR3 and subsequent trafficking of T cells to target tissues in allogeneic mouse models of GVHD [35]. Conversely, others have suggested that IFN-γ^+ $CD8^+$ T cells and IFN-γ^+ $CD4^+$ T cells are important in the initiation and progression of disease, respectively, in an allogeneic mouse model of GVHD [36]. Nevertheless, it remains to be determined if P2X7 functions through these mechanisms in allogeneic or humanized mouse models of GVHD.

The current study also identified the presence of serum hIL-17 in a small proportion of humanized mice (15-30%), and intracellular hIL-17 in an even smaller population of splenic $hCD4^+$ and $hCD8^+$ T cells (2-3%) from these mice. Due to the relatively small populations, it is not possible to positively determine the role of P2X7 on hIL-17 production in this

humanized mouse model of GVHD. However, the mean serum hIL-17 concentration was 10-fold greater in BBG-injected mice compared to saline-injected mice. These results may suggest P2X7 blockade promotes hIL-17 production in humanized mice, which contradicts previous *in vitro* results in which P2X7 activation promoted hIL-17 production in T cells [31]. Others have shown that a shift from an IFN-γ-producing to an IL-17-producing T cell phenotype exacerbates GVHD in an allogeneic mouse model of GVHD [37]. Similarly, increased numbers of IL-17-producing T cells were observed in patients with more severe GVHD [38]. Investigating IL-17-producing T cells at time points prior to end point or through increased sample sizes may assist in addressing the role of P2X7 blockade in IL-17 production in humanized mice with GVHD.

Due to the variation observed in hIL-17 mRNA expression between humanized mice, and the role of IL-1β in the differentiation of IL-17-producing T cells [39] including models of P2X7 activation [32], mIL-1β and hIL-1β was also examined in the current study. mIL-1β, but not hIL-1β, mRNA expression was detected in the livers and small intestines of humanized mice, with no differences observed between BBG- and saline-treatments. In contrast both mIL-1β and hIL-1β mRNA expression was detected in the spleens of humanized mice, with BBG treatment resulting in a 3-fold increase in mIL-1β mRNA expression and a 50% decrease in hIL-1β mRNA expression. However, there was no correlation between hIL-17 and hIL-1β, or between hIL-17 and mIL-1β mRNA expression (results not shown). Due to the inability to detect serum mIL-1β in these mice, serum mIL-1β could not be compared with serum hIL-17 (hIFN-γ). The inability to detect serum mIL-1β was not limited to this cytokine, as serum hIL-4 was not detected in initial experiments to establish the humanized mouse model, despite detection of serum hIFN-γ in these mice (results not shown).

As previously mentioned, injection of BBG into humanized mice did not alter disease progression, as assessed by weight loss, clinical score and survival. However, histological

examination revealed that BBG reduced the infiltration of leukocytes into the small intestine and skin in this humanized mouse model of GVHD. Moreover, there was also histological evidence of reduced tissue damage in these tissues from BBG-injected mice compared to saline-injected mice, observations supported by immunohistochemical analysis of T cell infiltrates and apoptosis. In contrast, BBG did not alter the proportion of $hCD4^+$ or $hCD8^+$ T cells in blood and spleens of humanized mice. Others have reported that humanized NSG mice exhibit leukocyte infiltration and tissue damage in the liver, small intestine and skin, characteristic of GVHD [40]. T cells are the main mediators of disease in this humanized mouse model of GVHD [41,42]. Consistent with these reports, immunohistochemical analysis with a human CD3 specific mAb detected T cells in the liver, small intestine and skin in humanized mice with GVHD. In support of this observation,hP2X7 mRNA was detected in the livers and small intestines of humanized mice using qPCR probes to the P2X7B splice variant, which is predominantly expressed in human T cells [43], with P2X7 present on both $hCD4^+$ and $hCD8^+$ T cells [44].

Collectively, the above data investigating the effect of the P2X7 antagonist, BBG, in a humanized mouse model of GVHD both confirms findings from previous studies using P2X7 antagonists in allogeneic mouse models of GVHD, and provides additional novel insights. Similar to allogeneic mouse models of GVHD [12-14], P2X7 antagonism reduced serum IFN-γ, immune infiltrates and tissue damage in humanized mice with GVHD. By contrast, no therapeutic benefit (weight loss, clinical score or survival) was observed in humanized mice with GVHD, but therapeutic benefits were observed in allogeneic mouse models of GVHD [12-14]. Besides obvious laboratory, species and mouse strain differences, a number of other notable differences remain between these models of GVHD. First, survival time in these allogeneic mouse models [12,13] is at least half that compared to humanized mice. Thus, extended or delayed injection regimes may be required to show therapeutic benefits in

humanized mice. Second, in the allogeneic mouse models, P2X7 antagonists were injected daily for the first 10 days [12,13] or twice weekly for 28 days [14] in contrast to five injections over the first 8 days in our humanized mouse model. Thus, more frequent or extended injection regimes may be required to show therapeutic benefits with BBG in humanized mice with GVHD. Third, the two studies that reported improved survival in the allogeneic mouse models [12,13] used the P2X7 antagonists, pyridoxal-phopshate-6-azophenyl-2',4-disulphonic acid, KN-62 or stavudine, rather than BBG. Thus, testing of P2X7 antagonists other than BBG in humanized mice with GVHD may be warranted. Although it should be noted that BBG at either 50 or 70 mg/kg (i.p. twice weekly for 28 days) prevented weight loss in one allogeneic mouse model of GVHD [14], indicating BBG can display some therapeutic benefit in this disease. Finally, in each of the allogeneic mouse models, recipient mice were first irradiated [12-14] , which causes ATP release [12]. In contrast, the humanized mice in our study were not irradiated, potentially eliminating this initial release of ATP, which may subsequently activate P2X7 to promote disease. Thus, the therapeutic potential of P2X7 antagonists in irradiated humanized mice with GVHD could be investigated.

Finally, this study showed that NSG mice demonstrate full-length functional P2X7. Firstly, qPCR revealed expression of *P2RX7* mRNA in the spleens, livers and small intestines of NSG mice. Secondly, immunoblotting revealed a major band at 81 kDa, correlating to glycosylated, full-length P2X7 [45]. Finally, ATP induced YO-PRO-1^{2+} uptake into splenic DCs from NSG mice, a process impaired by BBG, and which was absent in splenic DCs from P2X7 KO mice. ATP-induced YO-PRO-1^{2+} uptake into splenic DCs from NSG mice was significantly higher than splenic DCs from C57BL/6 mice. This is most likely due to the absence and presence of a loss-of-function mutation (P451L) [46] in NSG and C57BL/6 mice, respectively. Although it is yet to be formally demonstrated that NSG mice are wild-

type at this allele, NSG mice are derived from NOD mice [47], a strain known to encode a proline residue at amino acid position 451 [48].

In conclusion, the current study demonstrates P2X7 blockade with BBG can significantly reduce serum hIFN-γ, and inflammation and tissue damage in a humanized mouse model of GVHD. The similar clinical course with skewing to Th17 suggests that clinically P2X7 blockade may be of additive benefit if combined with strategies that limit Th17, such as IL-6 receptor blockade [49]. This study suggests a potential benefit for P2X7 blockade, but highlights the need to also address alternative pathways of immune activation.

ACKNOWLEDGEMENTS

This project was funded by the Illawarra Health and Medical Research Institute and the Centre for Medical and Molecular Biosciences (University of Wollongong). We would like to thank the technical staff of the Illawarra Health and Medical Research Institute, and the animal house staff at the Westmead Animal Facility for assistance. We would like to thank Professor David Steel (University of Wollongong) for statistical consulting.

DISCLOSURE

All authors declare that they have no disclosures.

AUTHOR CONTRIBUTIONS

N.J.G., L.B., D.L., S.R.A., S.I.A., M.S.S., R.S. and D.W. designed the experiments. N.J.G., L.B., D.L., S.R.A., V.S., R.S. and D.W. performed the experiments. N.J.G., L.B., D.L., S.R.A., R.S. and D.W. analyzed the data. S.F. and W.V. provided histological analysis. N.J.G. prepared the figures and wrote the manuscript. R.S. and D.W. edited the manuscript. L.B., D.L., S.R.A, S.F., W.V., M.S.S. and S.I.A. co-edited the manuscript.

REFERENCE LIST

1 Markey, K. A., MacDonald, K. P. A. & Hill, G. R. The biology of graft-versus-host disease: Experimental systems instructing clinical practice. Blood, 2014; **124:**354-362.

2 Jagasia, M., Arora, M., Flowers, M. E. D. *et al.* Risk factors for acute GVHD and survival after hematopoietic cell transplantation. Blood, 2012; **119:**296-307.

3 Ferrara, J. L., Levine, J. E., Reddy, P. & Holler, E. Graft-versus-host disease. The Lancet, 2009; **373:**1550-1561.

4 Yi, T., Chen, Y., Wang, L. *et al.* Reciprocal differentiation and tissue-specific pathogenesis of Th1, Th2, and Th17 cells in graft-versus-host disease. Blood, 2009; **114:**3101-3112.

5 Gartlan, K. H., Markey, K. A., Varelias, A. *et al.* Tc17 cells are a proinflammatory, plastic lineage of pathogenic CD8+ T cells that induce GVHD without antileukemic effects. Blood, 2015; **126:**1609-1620.

6 Holtan, S. G., Marcelo, P. & Weisdorf, D. J. Acute graft-versus-host disease: A bench-to-bedside update. Blood, 2014; **124:**363-373.

7 Cekic, C. & Linden, J. Purinergic regulation of the immune system. Nat. Rev. Immunol., 2016; **16:**177-192.

8 Junger, W. G. Immune cell regulation by autocrine purinergic signalling. Nature Reviews Immunology, 2011; **11:**201-212.

9 De Marchi, E., Orioli, E., Dal Ben, D. & Adinolfi, E. in *Adv. Protein Chem. Struct. Biol.* Vol. 104 39-79 (2016).

10 Geraghty, N. J., Watson, D., Adhikary, S. R. & Sluyter, R. P2X7 receptor in skin biology and diseases. World J Dermatol, 2016; **5:**72-83.

11 Wiley, J., Sluyter, R., Gu, B., Stokes, L. & Fuller, S. The human P2X7 receptor and its role in innate immunity. Tissue Antigens, 2011; **78:**321-332.

12 Wilhelm, K., Ganesan, J., Müller, T. *et al.* Graft-versus-host disease is enhanced by extracellular ATP activating P2X7R. Nat. Med., 2010; **16:**1434-1438.

13 Fowler, B. J., Gelfand, B. D., Kim, Y. *et al.* Nucleoside reverse transcriptase inhibitors possess intrinsic anti-inflammatory activity. Science, 2014; **346:**1000-1003.

14 Zhong, X., Zhu, F., Qiao, J., Zhao, K., Zhu, S., Zeng, L., Chen, X. & Xu, K. The impact of P2X7 receptor antagonist, brilliant blue G on graft-versus-host disease in mice after allogeneic hematopoietic stem cell transplantation. Cell. Immunol., 2016; **310:**71-77.

15 Lee, K.-H., Park, S. S., Kim, I. *et al.* P2X7 receptor polymorphism and clinical outcomes in HLA-matched sibling allogeneic hematopoietic stem cell transplantation. Haematologica, 2007; **92:**651-657.

16 Solle, M., Labasi, J., Perregaux, D. G., Stam, E., Petrushova, N., Koller, B. H., Griffiths, R. J. & Gabel, C. A. Altered cytokine production in mice lacking P2X7 receptors. J. Biol. Chem., 2001; **276:**125-132.

17 Tran, J. N., Pupovac, A., Taylor, R. M., Wiley, J. S., Byrne, S. N. & Sluyter, R. Murine epidermal Langerhans cells and keratinocytes express functional P2X7 receptors. Exp. Dermatol., 2010; **19:**e151-e157.

18 Bartlett, R., Yerbury, J. J. & Sluyter, R. P2X7 receptor activation induces reactive oxygen species formation and cell death in murine EOC13 microglia. Mediators Inflamm., 2013; **2013:**271813.

19 Spildrejorde, M., Bartlett, R., Stokes, L. *et al.* R270C polymorphism leads to loss of function of the canine P2X7 receptor. Physiol. Genomics, 2014; **46:**512-522.

20 King, M., Pearson, T., Shultz, L. D. *et al.* A new Hu-PBL model for the study of human islet alloreactivity based on NOD-*scid* mice bearing a targeted mutation in the IL-2 receptor gamma chain gene. Clin. Immunol., 2008; **126:**303-314.

21 Masin, M., Young, C., Lim, K. *et al.* Expression, assembly and function of novel C-terminal truncated variants of the mouse P2X7 receptor: Re-evaluation of P2X7 knockouts. Br. J. Pharmacol., 2012; **165:**978-993.

22 Matute, C., Torre, I., Pérez-Cerdá, F. *et al.* P2X7 receptor blockade prevents ATP excitotoxicity in oligodendrocytes and ameliorates experimental autoimmune encephalomyelitis. J. Neurosci., 2007; **27:**9525-9533.

23 Peng, W., Cotrina, M. L., Han, X. *et al.* Systemic administration of an antagonist of the ATP-sensitive receptor P2X7 improves recovery after spinal cord injury. Proc. Natl. Acad. Sci. U. S. A., 2009; **106:**12489-12493.

24 Díaz-Hernández, M., Díez-Zaera, M., Sánchez-Nogueiro, J., Gómez-Villafuertes, R., Canals, J. M., Alberch, J., Miras-Portugal, M. T. & Lucas, J. J. Altered P2X7-receptor level and function in mouse models of Huntington's disease and therapeutic efficacy of antagonist administration. FASEB J., 2009; **23:**1893-1906.

25 Bartlett, R., Stokes, L. & Sluyter, R. The P2X7 Receptor Channel: Recent Developments and the Use of P2X7 Antagonists in Models of Disease. Pharmacol. Rev., 2014; **66:**638-675.

26 Bartlett, R., Sluyter, V., Watson, D., Sluyter, R. & Yerbury, J. J. P2X7 antagonism using Brilliant Blue G reduces body weight loss and prolongs survival in female SOD1G93A amyotrophic lateral sclerosis mice. PeerJ, 2017; **5:**e3064.

27 Farrell, A. W., Gadeock, S., Pupovac, A., Wang, B., Jalilian, I., Ranson, M. & Sluyter, R. P2X7 receptor activation induces cell death and CD23 shedding in human RPMI 8226 multiple myeloma cells. Biochim. Biophys. Acta Gen. Subjects, 2010; **1800:**1173-1182.

28 Constantinescu, P., Wang, B., Kovacevic, K., Jalilian, I., Bosman, G. J. C. G. M., Wiley, J. S. & Sluyter, R. P2X7 receptor activation induces cell death and microparticle release in murine erythroleukemia cells. Biochimica et Biophysica Acta - Biomembranes, 2010; **1798:**1797-1804.

29 Englezou, P. C., Rothwell, S. W., Ainscough, J. S., Brough, D., Landsiedel, R., Verkhratsky, A., Kimber, I. & Dearman, R. J. P2X7R activation drives distinct IL-1 responses in dendritic cells compared to macrophages. Cytokine, 2015; **74:**293-304.

30 McCarthy Jr, P. L., Abhyankar, S., Neben, S., Newman, G., Sieff, C., Thompson, R. C., Burakoff, S. J. & Ferrara, J. L. M. Inhibition of interleukin-1 by an interleukin-1 receptor antagonist prevents graft-versus-host disease. Blood, 1991; **78:**1915-1918.

31 Ghiringhelli, F., Apetoh, L., Tesniere, A. *et al.* Activation of the NLRP3 inflammasome in dendritic cells induces IL-1β–dependent adaptive immunity against tumors. Nat. Med., 2009; **15:**1170-1178.

32 Zhao, J., Wang, H., Dai, C. *et al.* P2X7 blockade attenuates murine lupus nephritis by inhibiting activation of the NLRP3/ASC/Caspase 1 pathway. Arthritis Rheum., 2013; **65:**3176-3185.

33 Huang, J. J., Newton, R. C., Rutledge, S. J., Horuk, R., Matthew, J. B., Covington, M. & Lin, Y. Characterization of murine IL-1β: Isolation, expression, and purification. J. Immunol., 1988; **140:**3838-3843.

34 Vandenabeele, P., Declercq, W., Libert, C. & Fiers, W. Development of a simple, sensitive and specific bioassay for interleukin-1 based on the proliferation of RPMI 1788 cells comparison with other bioassays for IL-1. J. Immunol. Methods, 1990; **135:**25-32.

35 Choi, J., Ziga, E. D., Ritchey, J., Collins, L., Prior, J. L., Cooper, M. L., Piwnica-Worms, D. & DiPersio, J. F. IFNγR signaling mediates alloreactive T-cell trafficking and GVHD. Blood, 2012; **120:**4093-4103.

36 Zhao, K., Ruan, S., Yin, L. *et al.* Dynamic regulation of effector IFN-γ-producing and IL-17-producing T cell subsets in the development of acute graft-versus-host disease. Mol. Med. Report., 2016; **13:**1395-1403.

37 Pan, B., Zeng, L., Cheng, H., Song, G., Chen, C., Zhang, Y., Li, Z. & Xu, K. Altered balance between Th1 and Th17 cells in circulation is an indicator for the severity of murine acute GVHD. Immunol. Lett., 2012; **142:**48-54.

38 Zhao, X. Y., Xu, L. L., Lu, S. Y. & Huang, X. J. IL-17-producing T cells contribute to acute graft-versus-host disease in patients undergoing unmanipulated blood and marrow transplantation. Eur. J. Immunol., 2011; **41:**514-526.

39 Acosta-Rodriguez, E. V., Napolitani, G., Lanzavecchia, A. & Sallusto, F. Interleukins 1[beta] and 6 but not transforming growth factor-[beta] are essential for the differentiation of interleukin 17-producing human T helper cells. Nat. Immunol., 2007; **8:**942-949.

40 King, M., Covassin, L., Brehm, M. *et al.* Human peripheral blood leucocyte non-obese diabetic-severe combined immunodeficiency interleukin-2 receptor gamma chain gene mouse model of xenogeneic graft-versus-host-like disease and the role of host major histocompatibility complex. Clin. Exp. Immunol., 2009; **157:**104-118.

41 Covassin, L., Jangalwe, S., Jouvet, N., Laning, J., Burzenski, L., Shultz, L. D. & Brehm, M. A. Human immune system development and survival of non-obese diabetic (NOD)-scid IL2rγnull (NSG) mice engrafted with human thymus and autologous haematopoietic stem cells. Clin. Exp. Immunol., 2013; **174:**372-388.

42 Abraham, S., Choi, J. G., Ye, C., Manjunath, N. & Shankar, P. IL-10 exacerbates xenogeneic GVHD by inducing massive human T cell expansion. Clin. Immunol., 2015; **156:**58.

43 Adinolfi, E., Cirillo, M., Woltersdorf, R. *et al.* Trophic activity of a naturally occurring truncated isoform of the P2X7 receptor. FASEB J., 2010; **24:**3393-3404.

44 Sluyter, R. & Wiley, J. S. P2X7 receptor activation induces CD62L shedding from human CD4+ and CD8+ T cells. Inflamm Cell Signal, 2014; **1:**e92.

45 Pupovac, A., Geraghty, N. J., Watson, D. & Sluyter, R. Activation of the P2X7 receptor induces the rapid shedding of CD23 from human and murine B cells. Immunol. Cell Biol., 2014; **93:**77-85.

46 Adriouch, S., Dox, C., Welge, V., Seman, M., Koch-Nolte, F. & Haag, F. Cutting edge: A natural P451L mutation in the cytoplasmic domain impairs the function of the mouse P2X7 receptor. J. Immunol., 2002; **169:**4108-4112.

47 Shultz, L. D., Ishikawa, F. & Greiner, D. L. Humanized mice in translational biomedical research. Nature Reviews Immunology, 2007; **7:**118-130.

48 Syberg, S., Schwarz, P., Petersen, S., Steinberg, T. H., Jensen, J. E. B., Teilmann, J. & Jorgensen, N. R. Association between P2X7 receptor polymorphisms and bone status in mice. J Osteoporos, 2012; **2012:**

49 Chen, X., Das, R., Komorowski, R., Beres, A., Hessner, M. J., Mihara, M. & Drobyski, W. R. Blockade of interleukin-6 signaling augments regulatory T-cell reconstitution and attenuates the severity of graft-versus-host disease. Blood, 2009; **114:**891-900.

FIGURE LEGENDS

Fig. 1. Engraftment of human leukocytes and development of GVHD in NOD-SCID-IL2Rγ^{null} (NSG) mice.

(a-g) NSG mice were injected intra-peritoneally (i.p.) with either 10 x 10^6 human (h) peripheral blood mononuclear cells (PBMCs) (n = 9) or an equal volume of saline (control) (n = 9), and monitored for clinical signs of graft-versus-host disease (GVHD) over 8 weeks. (a-g) The percentage of human leukocytes in (a-c) blood at 3 weeks post-hPBMC injection and (d-f) spleens at end point were determined by flow cytometry. (a, d) hCD45$^+$ leukocytes are expressed as a percentage of total mCD45$^+$ and hCD45$^+$ leukocytes. (b, e) hCD3$^+$ hCD19$^-$ cells and (c, f) hCD3$^-$ hCD19$^-$ cells are expressed as a percentage of total hCD45$^+$ leukocytes. (g) hCD4$^+$ and hCD8$^+$ T cell subsets are expressed as a percentage of total hCD3$^+$ leukocytes. Data represents group means ± SEM; symbols represent individual mice; * $P < 0.05$ compared to hCD8$^+$ T cells. (h-j) NSG mice were monitored for (h) weight loss, (i) clinical score and (j) survival. Data represents (h, i) group means ± SEM, or (j) percent survival (control, n = 9, hPBMC n = 9); * $P < 0.05$ and ** $P < 0.005$ compared to control mice.

Fig. 2. NOD-SCID-IL2Rγ^{null} (NSG) mice injected with human leukocytes develop graft-versus-host disease (GVHD).

(a-d) NSG mice injected intra-peritoneally (i.p.) with either human (h) peripheral blood mononuclear cells (hPBMCs) or saline (control) (day 0) (from Fig. 1) were monitored for clinical signs of graft-versus-host disease (GVHD) over 8 weeks. (a) Tissue sections (liver, small intestine and skin) from control (top panel) or hPBMC-injected mice (bottom panel) at end point were stained with haematoxylin and eosin and captured by microscopy. Each image

is representative of two mice per group; bar represents 100 μm. (b-d) The relative expression of murine (m) P2X7 in (b) spleen, (c) liver and (d) small intestine from mice at end point was examined by qPCR. Data represents group means ± SEM (n = 4-7); symbols represent individual mice.

Fig. 3. NOD-SCID-IL2Rγ^{null} (NSG) mice express full-length functional P2X7.

(a) Lysates of RAW264.7 (RAW) macrophages and splenocytes from NSG mice were examined by immunoblotting using an anti-P2X7 antibody. Image is representative of two independent experiments. (b) RAW264.7 cells or splenocytes from C57BL/6, P2X7 KO or NSG mice in NaCl medium containing 1 μM YO-PRO-1^{2+} were incubated in the absence or presence of 1 mM adenosine triphosphate (ATP) for 10 min at 37°C. The mean fluorescence intensity of YO-PRO-1^{2+} uptake into RAW264.7 cells or CD11c^{+} splenic dendritic cells (DCs) was then assessed by flow cytometry. ATP-induced YO-PRO-1^{2+} uptake was determined as the difference between YO-PRO-1^{2+} uptake in the presence and absence of ATP. Data represents group means ± SEM (n = 3 - 5); symbols represent individual replicates (RAW264.7 cells) or mice (splenic CD11c^{+} DCs); ** P < 0.005 and *** P < 0.0001 compared to C57BL/6.

Fig. 4. Brilliant Blue G (BBG) prevents adenosine triphosphate (ATP)-induced cation uptake into human and murine leukocytes.

(a) Human RPMI8226 and murine RAW264.7 cells, (b) human peripheral blood mononuclear cells (PBMCs) or (c) NOD-SCID-IL2Rγ^{null} (NSG) splenocytes in NaCl medium were pre-incubated for 15 min at 37°C in the absence or presence of (a) BBG as indicated or (b, c) 1 μM BBG. Cells were then incubated with 1 μM YO-PRO-1^{2+} in the absence or

presence of 1 mM adenosine triphosphate (ATP) for 10 min at 37°C. The mean fluorescence intensity of YO-PRO-1^{2+} uptake into (a) RPMI8226 or RAW264.7 cells, (b) $hCD3^+$ T cells or (b) NSG splenic $CD11c^+$ dendritic cells (DCs) was then assessed by flow cytometry. (a) ATP-induced YO-PRO-1^{2+} uptake is represented as a percentage of maximal ATP response in the absence of BBG. (a-c) Data represents group means ± SEM (n = 3); *** $P < 0.0001$ compared to respective basal.

Fig. 5. Brilliant Blue G (BBG) does not affect engraftment of human cells.

(a-j) NOD-SCID-IL2Rγ^{null} (NSG) mice were injected intra-peritoneally (i.p.) with 10 x 10^6 human (h) peripheral blood mononuclear cells (PBMCs), and subsequently with saline (control) (n = 14) or saline containing Brilliant Blue G (BBG) (50 mg/kg) (n = 16) every two days (from days 0-8), and monitored for clinical signs of graft-versus-host disease (GVHD) over 10 weeks. (a-g) The percentage of human leukocytes in (a-c) blood at 3 weeks post-hPBMC injection and (d-f) spleens at end point were determined by flow cytometry. (a, d) $hCD45^+$ leukocytes are expressed as a percentage of total $mCD45^+$ and $hCD45^+$ leukocytes. (b, e) $hCD3^+$ $hCD19^-$ cells and (c, f) $hCD3^-$ $hCD19^-$ cells are expressed as a percentage of total $hCD45^+$ leukocytes. (g) $hCD4^+$ and $hCD8^+$ T cell subsets are expressed as a percentage of total $hCD3^+$ leukocytes. Data represents group means ± SEM; symbols represent individual mice; *** $P < 0.0001$ compared to $hCD8^+$ T cells. (h-j) NSG mice were monitored for (a) weight loss, (b) clinical score, and (c) survival. Data represents (h, i) group means ± SEM or (j) percent survival (saline n = 14, BBG n = 16).

Fig. 6. Brilliant Blue G (BBG) does not prevent graft-versus-host disease (GVHD) in humanized mice.

(a-c) NOD-SCID-IL2Rγ^{null} (NSG) mice injected intra-peritoneally (i.p.) with 10 x 10^6 human (h) peripheral blood mononuclear cells (PBMCs) (day 0), and with saline (control) or 50 mg/kg Brilliant Blue G (BBG) (from Fig. 5) were monitored for clinical signs of GVHD over 10 weeks. Tissue sections (liver, small intestine, and skin) from hPBMC-injected mice injected with saline (control) or BBG at end point were stained with (a) haematoxylin and eosin, (b) anti-hCD3 monoclonal antibody with 3,3'-diaminobenzidine tetrachloride detection system and haematoxylin, or (c) terminal deoxynucleotidyl transferase deoxyuridine triphosphate nick-end labelling with 3,3'-diaminobenzidine tetrachloride detection system and methyl green. Images were captured by microscopy with each image representative of (a) four, or (b, c) two mice per group; bars represent 100 μm; (b) black arrow heads indicate T cells, and (c) red arrow heads indicate apoptotic cells.

Fig. 7. Brilliant Blue G (BBG) does not impact expression of mP2X7 or hP2X7 in tissues in humanized mice.

(a-f) NOD-SCID-IL2Rγ^{null} (NSG) mice injected intra-peritoneally (i.p.) with 10 x 10^6 human peripheral blood mononuclear cells (day 0), and with saline (control) or 50 mg/kg Brilliant Blue G (BBG) (from Fig. 5) were monitored for clinical signs of GVHD over 10 weeks. The relative expression of (a-c) murine (m) P2X7 and (d-f) hP2X7 in (a, d) spleen, (b, e) liver, and (c, f) small intestine from mice at end point were examined by qPCR. Data represents group means ± SEM (n = 4-6); symbols represent individual mice.

Fig. 8. Brilliant Blue G (BBG) significantly reduces serum human interferon (IFN)-γ in humanized mice.

(a-j) NOD-SCID-IL2Rγ^{null} (NSG) mice were injected intra-peritoneally (i.p.) with 10 x 10^6 human (h) peripheral blood mononuclear cells (PBMCs) (day 0), and with saline (control) or 50 mg/kg Brilliant Blue G (BBG) (from Fig. 5). Concentrations of serum (a) hIFN-γ, and (b) hIL-17 were analyzed by ELISA. Data represents group means ± SEM (saline n = 12, BBG n = 13); $^{**}P < 0.005$ compared to saline-injected mice. (c, d) Splenocytes were incubated in complete RPMI 1640 medium containing phorbol 12-myristate 13-acetate and ionomycin for 4 h, and the percentage of hCD4$^+$ and hCD8$^+$ T cells producing intracellular (c) hIFN-γ or (d) hIL-17 was determined by flow cytometry. Data represents group means ± SEM (saline n = 3, BBG = 4); symbols represent individual mice; $^{*}P < 0.05$ compared to corresponding hCD4$^+$ T cells. (e-j) The relative expression of (e-g) hIFN-γ and (h-j) hIL-17 in (e, h) spleen, (f, i) liver and (g, j) small intestine from mice at end point were examined by qPCR. Data represents group means ± SEM (n = 2-6); symbols represent individual mice. ND = not detected.

Fig. 9. Brilliant Blue G (BBG) does not alter relative expression of human or murine IL-1β in humanized mice.

(a-d) NOD-SCID-IL2Rγ^{null} (NSG) mice were injected intra-peritoneally (i.p.) with 10 x 10^6 human (h) peripheral blood mononuclear cells (PBMCs) (day 0), and with saline (control) or 50 mg/kg Brilliant Blue G (BBG) (from Fig. 5). The relative expression of (a-c) murine (m) interleukin (IL)-1β and (d) hIL-1β in (a, d) spleen, (b) liver and (c) small intestine from mice at end point were examined by qPCR. Data represents group means ± SEM (n = 3-6); symbols represent individual mice.

SUPPLEMENTARY FIGURES

Fig. S1. Flow cytometric gating of leukocytes in blood from humanized mice

Blood cells from humanized mice were labelled with isotype control or CD-specific monoclonal antibodies (mAb). Forward and side scatter was used to identify leukocytes, which were subsequently used to identify human leukocytes ($hCD45^+$ $mCD45^-$), human T cells ($hCD45^+$ $mCD45^-$ $hCD3^+$ $hCD19^-$) and human B cells ($hCD45^+$ $mCD45^-$ $hCD3^-$ $hCD19^+$).

Fig. S2. Flow cytometric gating of leukocytes in spleens from humanized mice

Splenocytes from humanized mice were labelled with isotype control or CD-specific monoclonal antibodies (mAb). Forward and side scatter was used to identify leukocytes, which were subsequently used to identify human leukocytes ($hCD45^+$ $mCD45^-$), human T cells ($hCD45^+$ $mCD45^-$ $hCD3^+$ $hCD19^-$) and human B cells ($hCD45^+$ $mCD45^-$ $hCD3^-$ $hCD19^+$). Forward and side scatter was used to identify leukocytes, which were subsequently used to identify human $CD4^+$ T cell ($hCD3^+$ $hCD4^+$ $hCD8^-$), and human $hCD8^+$ T cell ($hCD3^+$ $hCD4^-$ $hCD8^+$) subsets.

Fig. S3. Flow cytometric analysis of YO-PRO-1^{2+} uptake into human $hCD3^+$ T cells and $CD11c^+$ splenic dendritic cells.

Human PBMCs and splenocytes from NOD-SCID-IL2Rγ^{null} mice were incubated with YO-PRO-1^{2+} in the absence (basal) (grey histograms) or presence of adenosine triphosphate (ATP) (black histograms), and subsequently labelled with anti-human (h) CD3 or anti-murine (m) CD11c monoclonal antibody. Forward and side scatter was used to identify leukocytes, which were subsequently used to identify $hCD3^+$ T cells or murine $CD11c^+$ splenic DCs. YO-PRO-1^{2+} uptake into these cells was then quantified using geometric mean fluorescence of histograms.

Fig. S4. Flow cytometric analysis of intracellular human IFN-γ and IL-17 in human $CD4^+$ and $CD8^+$ T cells

Splenocytes from humanized mice were incubated with phorbol 12-myristate 13-acetate and ionomycin, and labelled with isotype control or specific monoclonal antibodies. Forward and side scatter was used to identify leukocytes, which were subsequently used to identify human $CD4^+$ T cell ($hCD3^+$ $hCD4^+$ $hCD8^-$), and human $hCD8^+$ T cell ($hCD3^+$ $hCD4^-$ $hCD8^+$) subsets. The percentage of hIFN-γ and hIL-17 was quantified as the difference between cytokine specific (black histograms) and isotype control (grey histograms) mAb labelling (indicated by marker regions as shown).

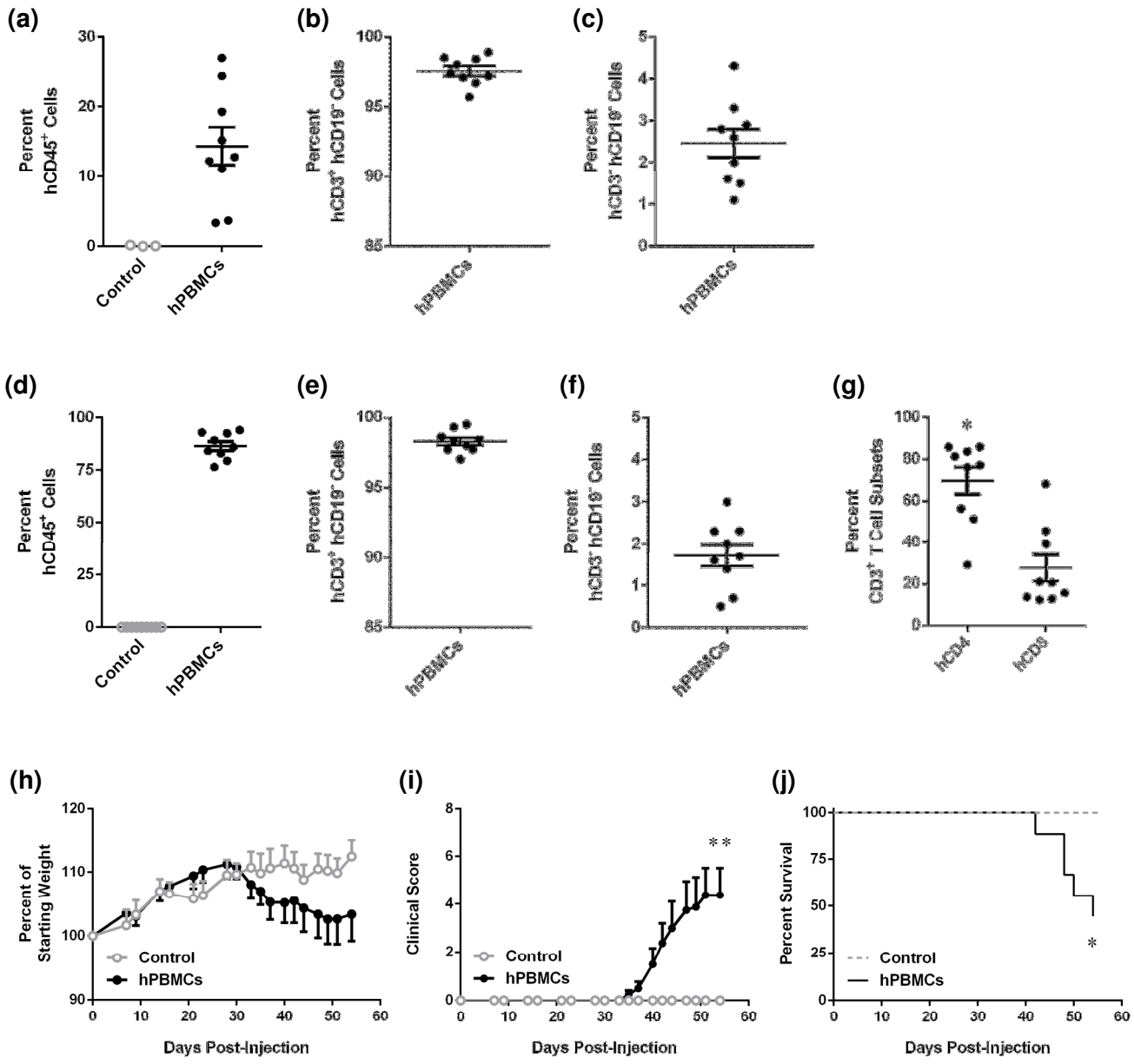
(a)
Percent hCD45+ Cells
Control
hPBMCs
(b)
Percent hCD3+ hCD19- Cells
hPBMCs
(c)
Percent hCD3+ hCD19- Cells
hPBMCs
(d)
Percent hCD45+ Cells
Control
hPBMCs
(e)
Percent hCD3+ hCD19- Cells
hPBMCs
(f)
Percent hCD3+ hCD19- Cells
hPBMCs
(g)
Percent CD3+ T Cell Subsets
hCD4
hCD8
(h)
Percent of Starting Weight
Control
hPBMCs
Days Post-Injection
(i)
Clinical Score
Control
hPBMCs
Days Post-Injection
(j)
Percent Survival
Control
hPBMCs
Days Post-Injection

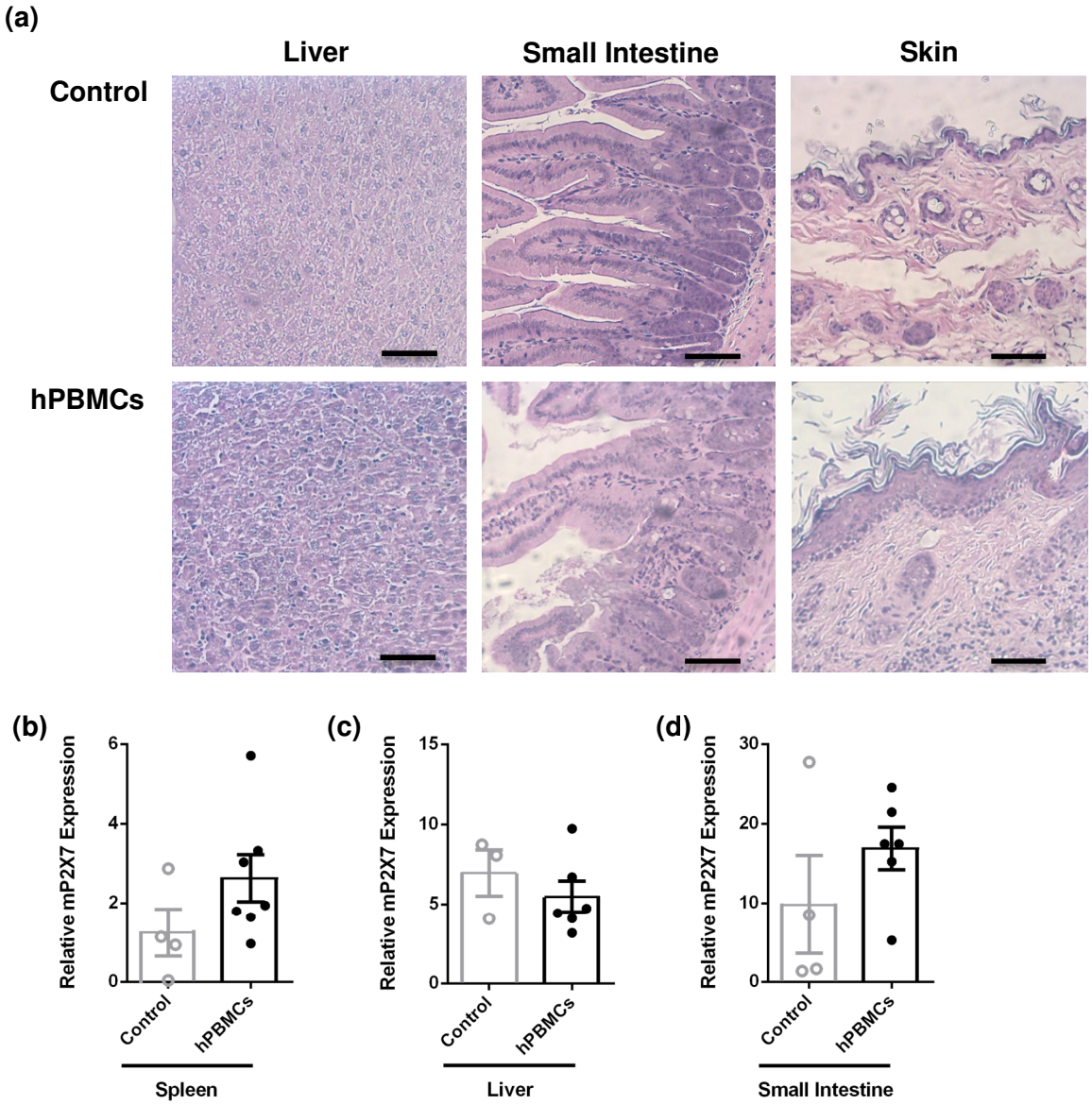
(a)
Liver
Small Intestine
Skin
Control
hPBMCs
(b)
Relative mP2X7 Expression
0
2
4
6
Control
hPBMCs
Spleen
(c)
Relative mP2X7 Expression
0
5
10
15
Control
hPBMCs
Liver
(d)
Relative mP2X7 Expression
0
10
20
30
Control
hPBMCs
Small Intestine

(a)

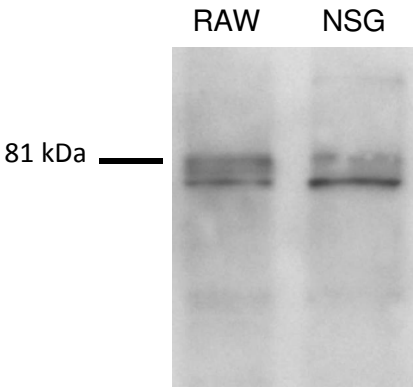
RAW
NSG
81 kDa

(b)

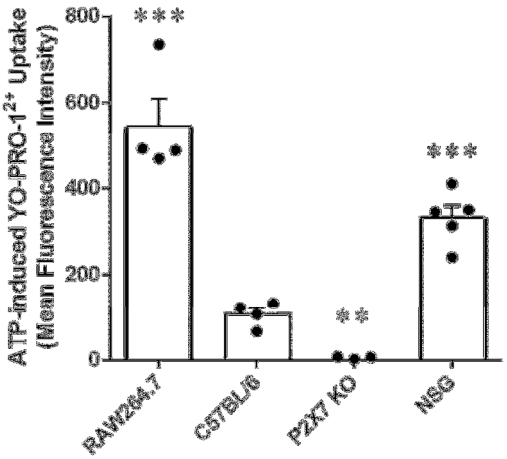
ATP-induced YO-PRO-1^{2+} Uptake
(Mean Fluorescence Intensity)
800
600
400
200
0
***
**
***
RAW264.7
C57BL/6
P2X7 KO
NSG

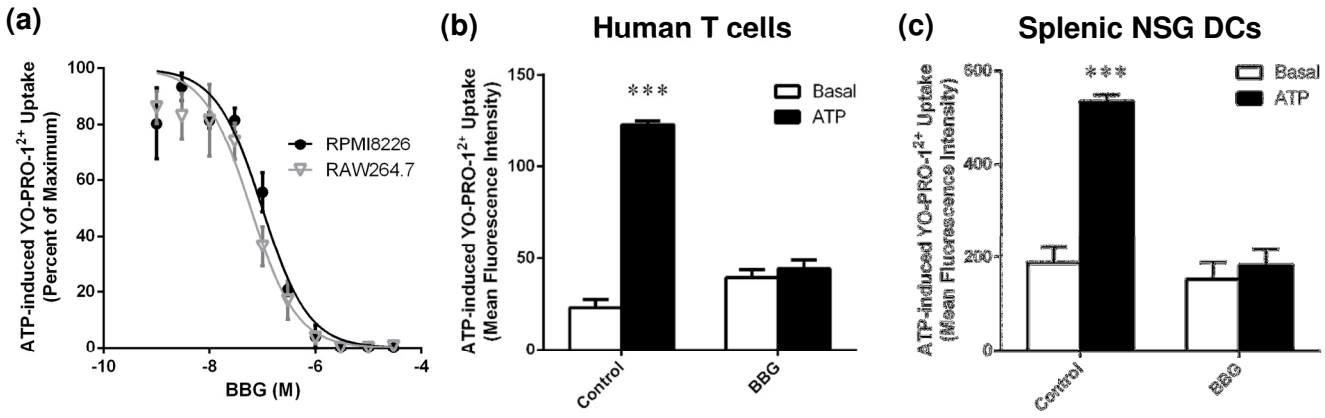
(a)
ATP-induced YO-PRO-1^{2+} Uptake
(Percent of Maximum)
100
80
60
40
20
0
-10
-8
-6
-4
BBG (M)
RPMI8226
RAW264.7
(b)
Human T cells
ATP-induced YO-PRO-1^{2+} Uptake
(Mean Fluorescence Intensity)
150
100
50
0
***
Basal
ATP
Control
BBG
(c)
Splenic NSG DCs
ATP-induced YO-PRO-1^{2+} Uptake
(Mean Fluorescence Intensity)
600
400
200
0
***
Basal
ATP
Control
BBG

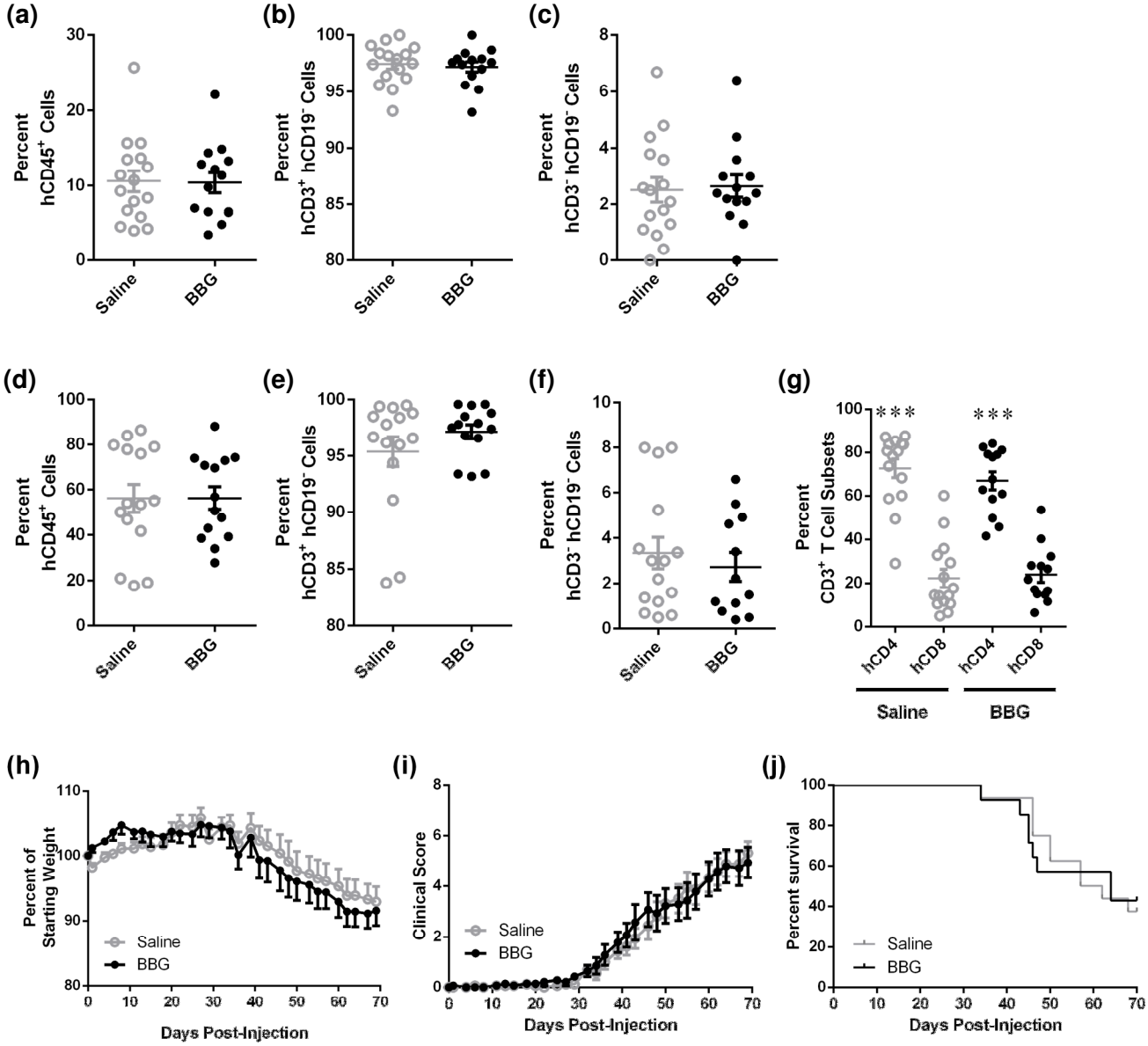
(a)
Percent hCD45+ Cells
Saline
BBG
(b)
Percent hCD3+ hCD19- Cells
(c)
Percent hCD3- hCD19- Cells
(d)
(e)
(f)
(g)
Percent CD3+ T Cell Subsets
***
hCD4
hCD8
(h)
Percent of Starting Weight
Days Post-Injection
(i)
Clinical Score
(j)
Percent survival

(a)

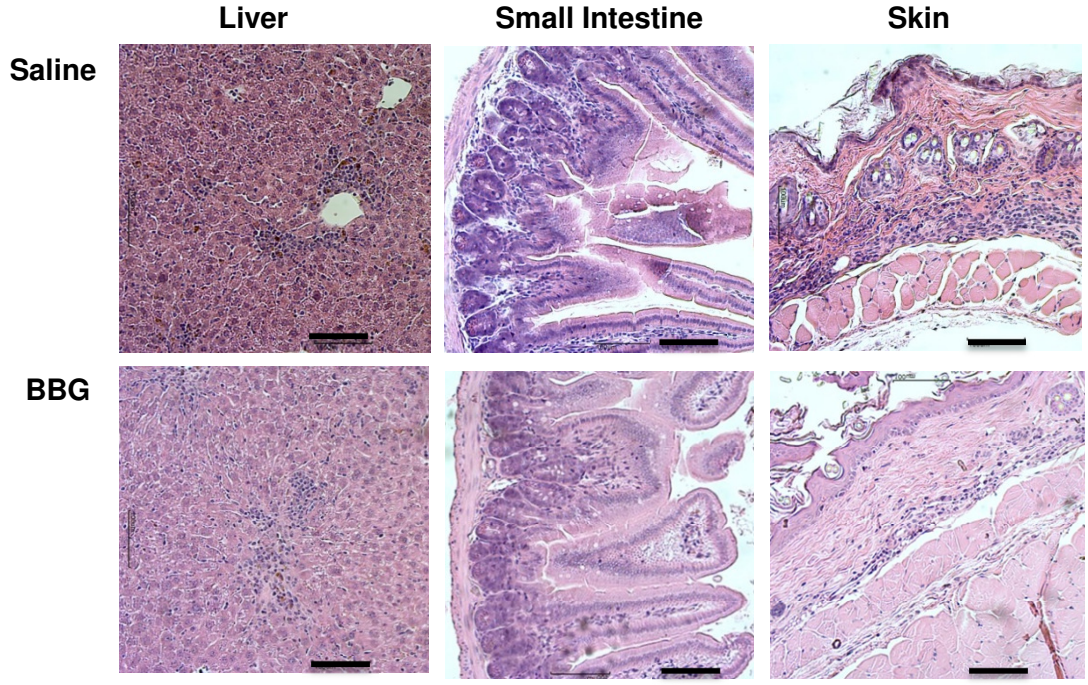
Liver
Small Intestine
Skin
Saline
BBG

(b)

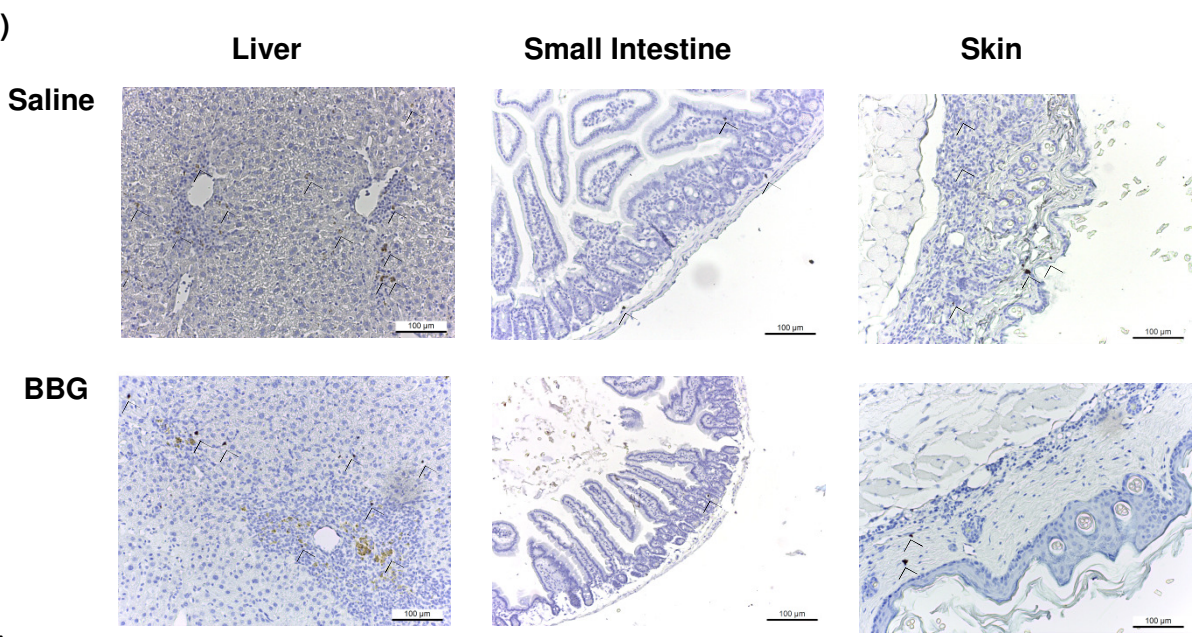
Liver
Small Intestine
Skin
Saline
BBG

(c)

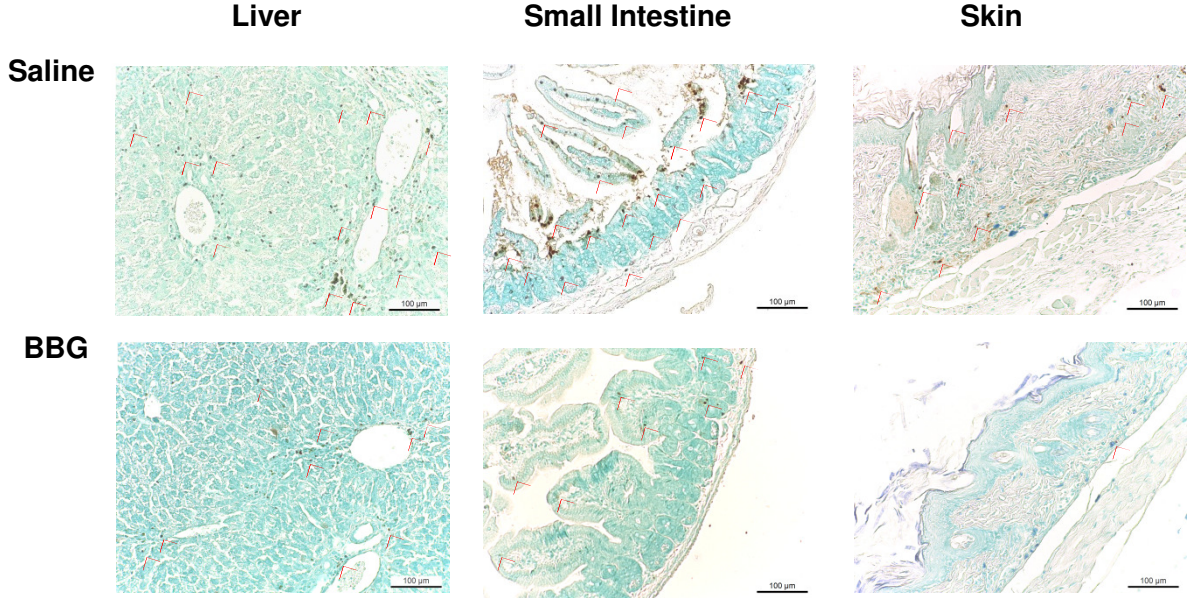
Liver
Small Intestine
Skin
Saline
BBG

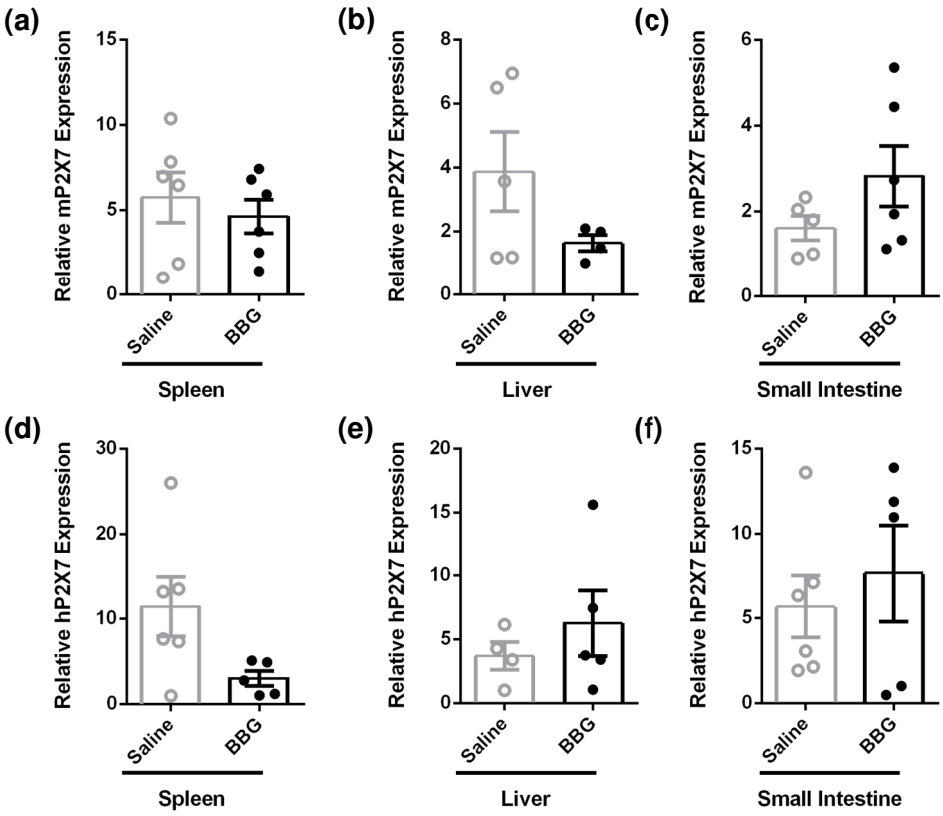
(a)
Relative mP2X7 Expression
15
10
5
0
Saline
BBG
Spleen
(b)
Relative mP2X7 Expression
8
6
4
2
0
Saline
BBG
Liver
(c)
Relative mP2X7 Expression
6
4
2
0
Saline
BBG
Small Intestine
(d)
Relative hP2X7 Expression
30
20
10
0
Saline
BBG
Spleen
(e)
Relative hP2X7 Expression
20
15
10
5
0
Saline
BBG
Liver
(f)
Relative hP2X7 Expression
15
10
5
0
Saline
BBG
Small Intestine

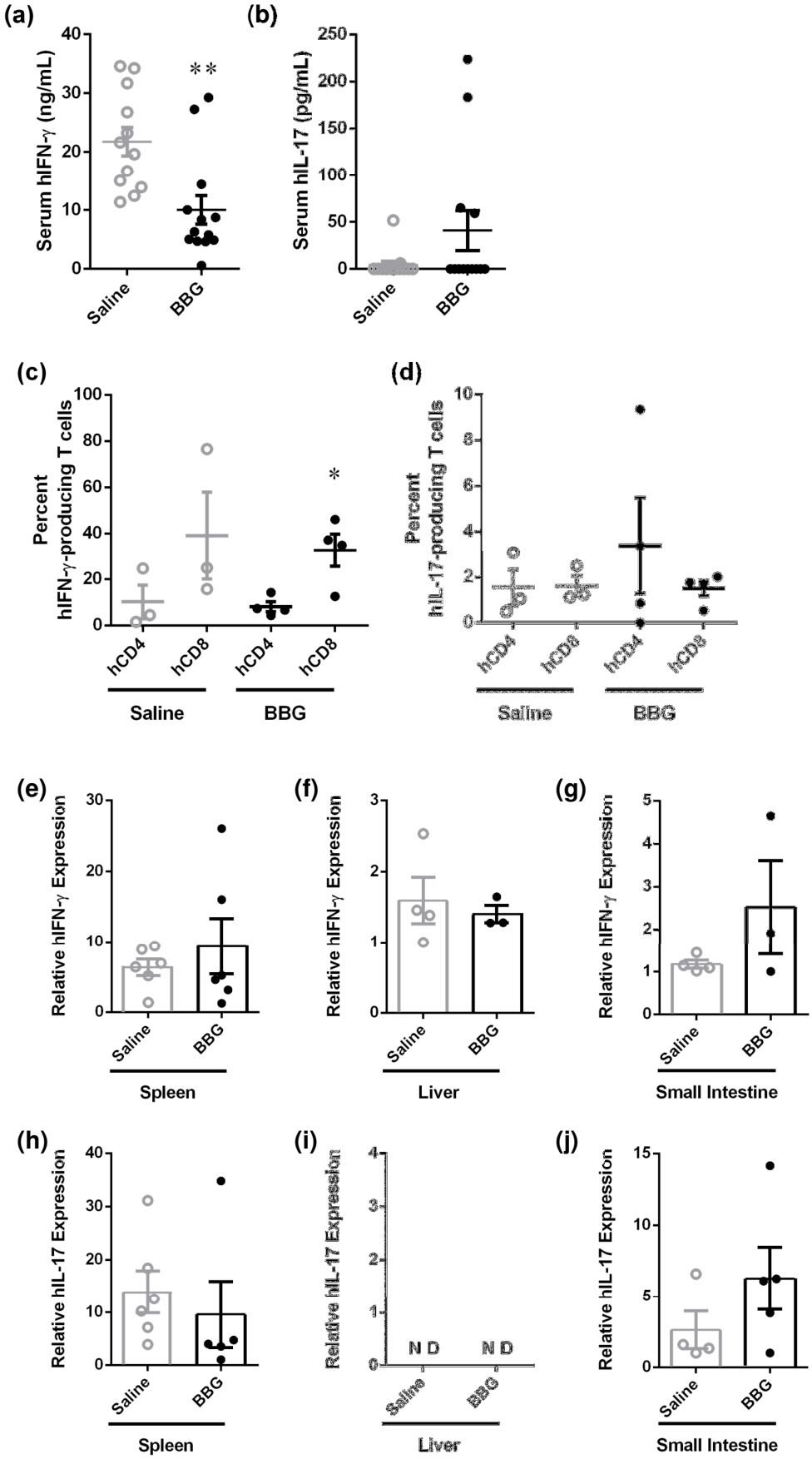
(a)
Serum hIFN-γ (ng/mL)
40
30
20
10
0
**
Saline
BBG
(b)
Serum hIL-17 (pg/mL)
250
200
150
100
50
0
Saline
BBG
(c)
Percent hIFN-γ-producing T cells
100
80
60
40
20
0
*
hCD4
hCD8
hCD4
hCD8
Saline
BBG
(d)
Percent hIL-17-producing T cells
10
8
6
4
2
0
hCD4
hCD8
hCD4
hCD8
Saline
BBG
(e)
Relative hIFN-γ Expression
30
20
10
0
Saline
BBG
Spleen
(f)
Relative hIFN-γ Expression
3
2
1
0
Saline
BBG
Liver
(g)
Relative hIFN-γ Expression
5
4
3
2
1
0
Saline
BBG
Small Intestine
(h)
Relative hIL-17 Expression
40
30
20
10
0
Saline
BBG
Spleen
(i)
Relative hIL-17 Expression
4
3
2
1
0
N D
N D
Saline
BBG
Liver
(j)
Relative hIL-17 Expression
15
10
5
0
Saline
BBG
Small Intestine

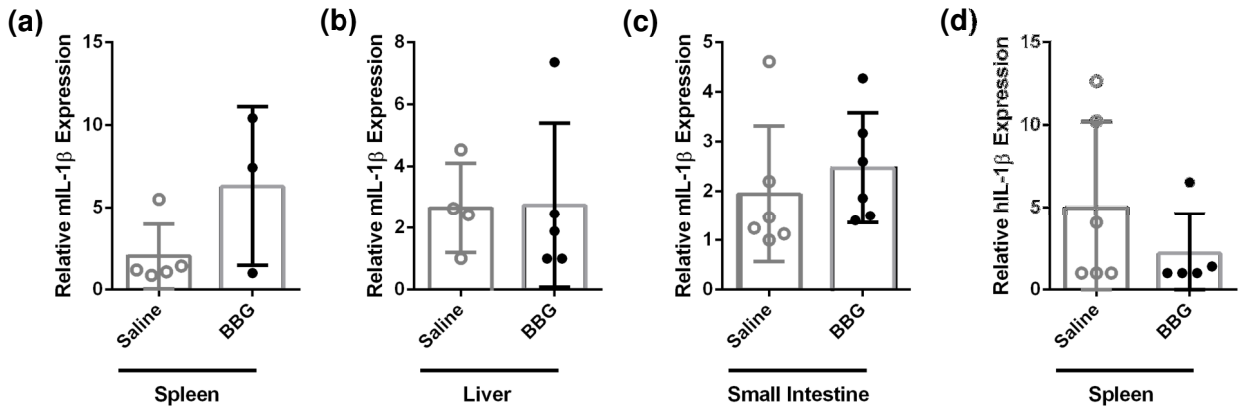
(a)
Relative mIL-1β Expression
15
10
5
0
Saline
BBG
Spleen
(b)
Relative mIL-1β Expression
8
6
4
2
0
Saline
BBG
Liver
(c)
Relative mIL-1β Expression
5
4
3
2
1
0
Saline
BBG
Small Intestine
(d)
Relative hIL-1β Expression
15
10
5
0
Saline
BBG
Spleen

Fig. S1

Isotype control mAb

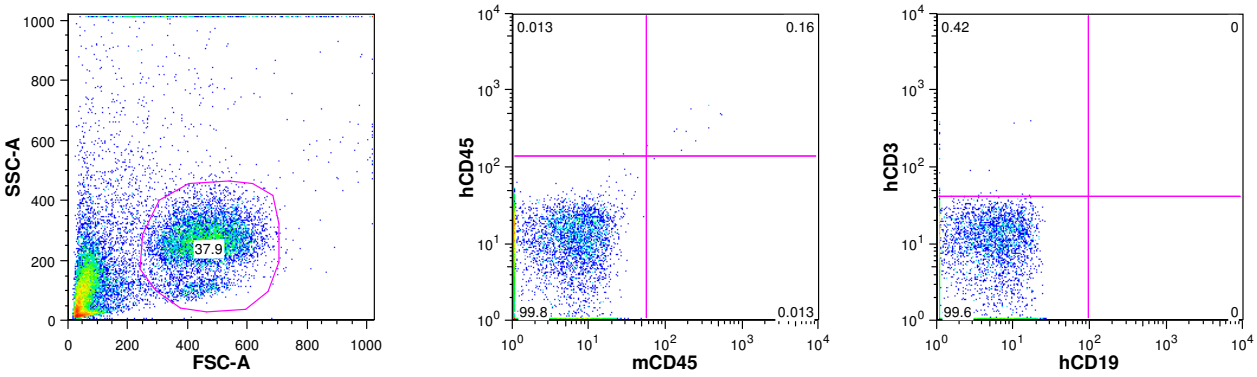

CD specific mAb

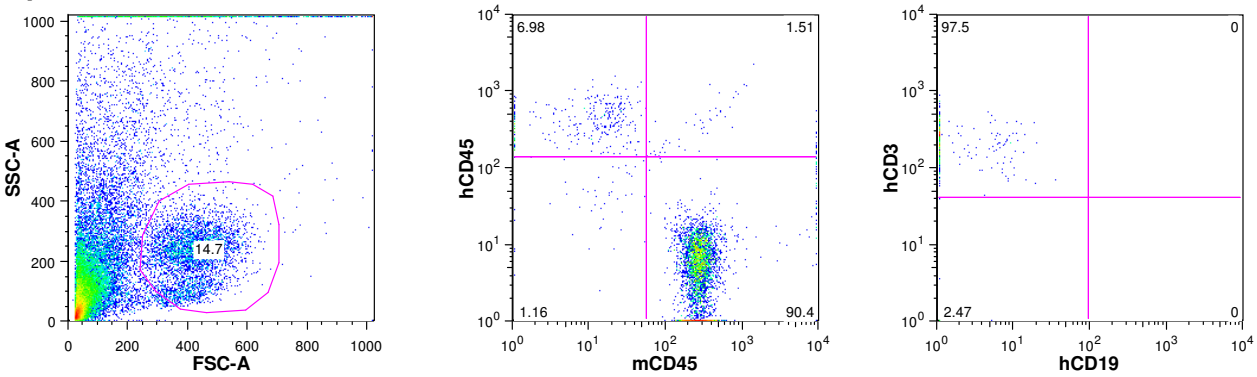

Fig. S2

Isotype control mAb

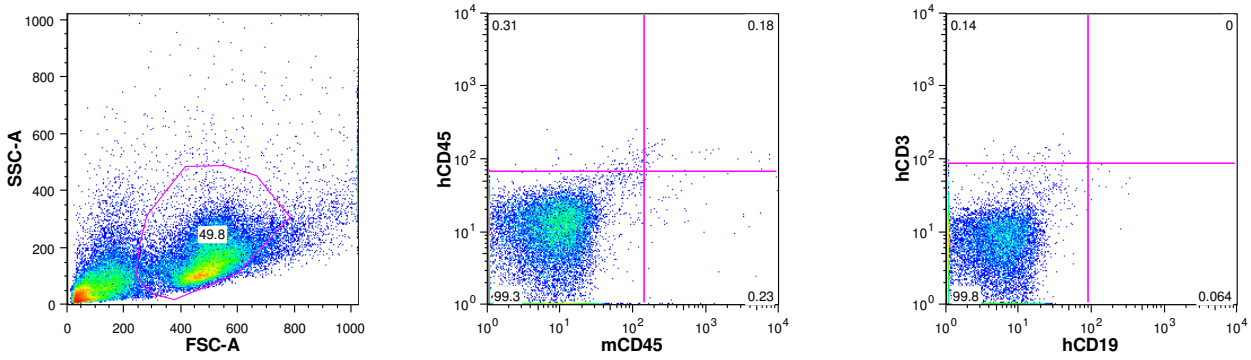

CD specific mAb

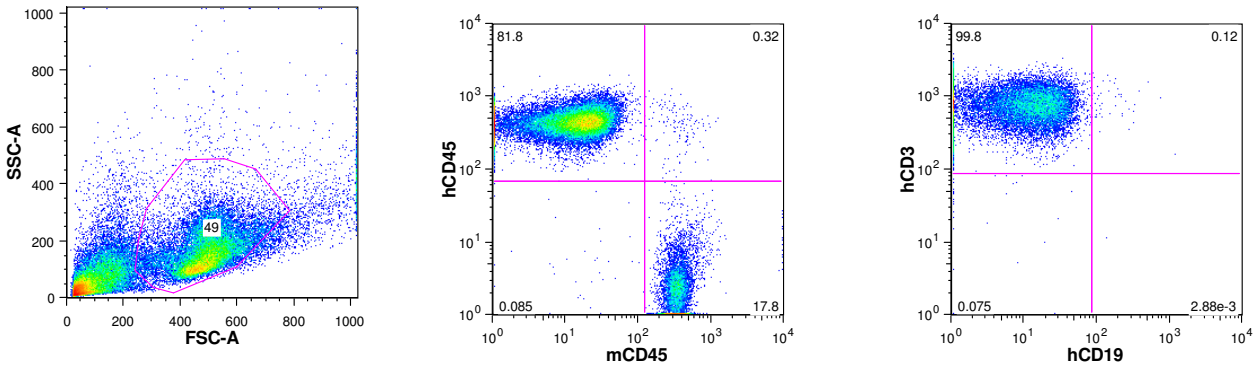

Isotype control mAb

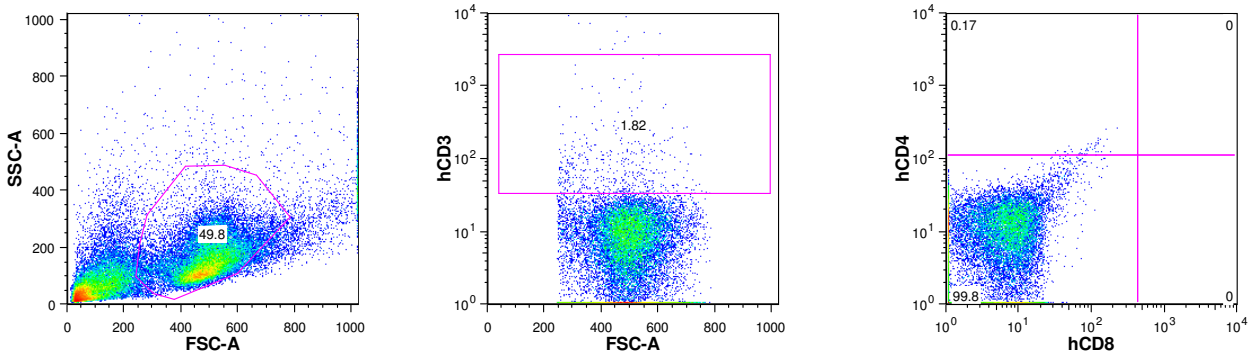

CD specific mAb

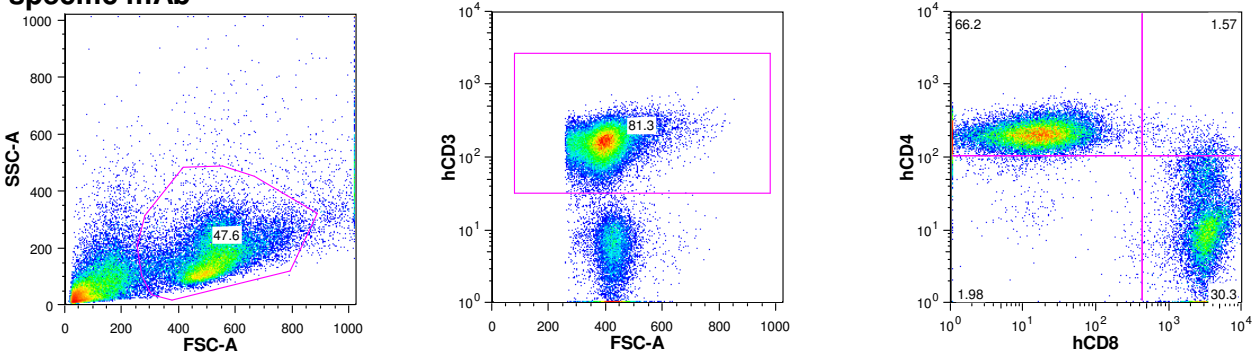

Fig. S3

Human T Cells

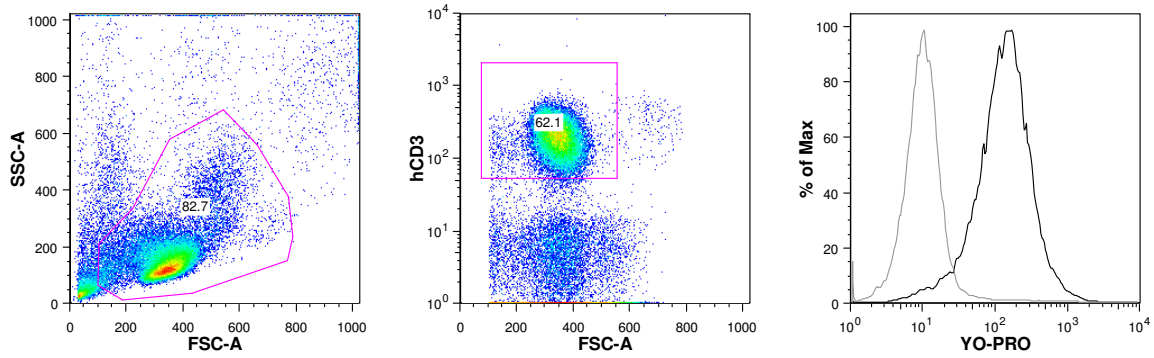

Splenic NSG DCs

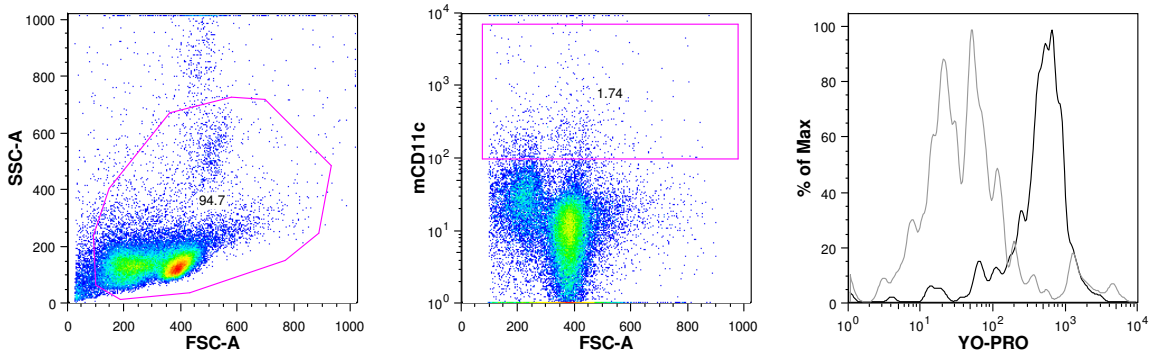

Fig. S4

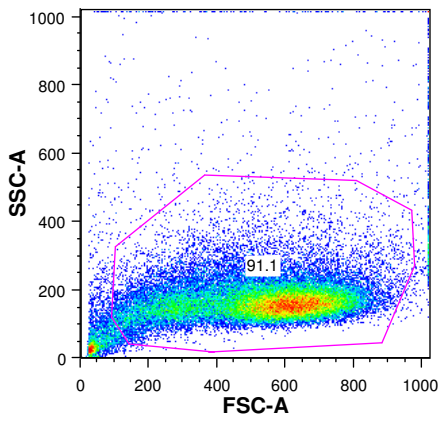

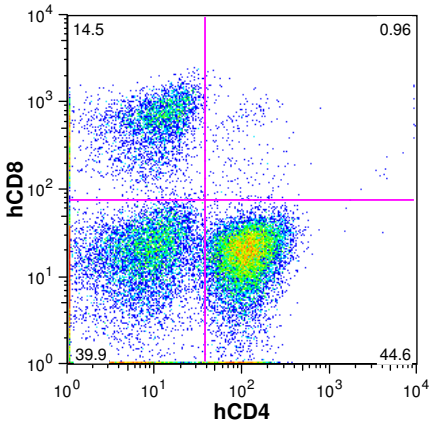

CD4$^+$ T cells

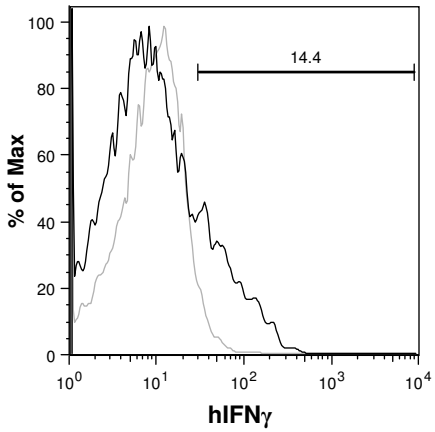

CD8$^+$ T cells

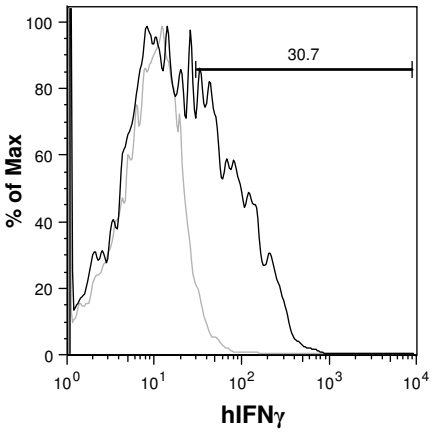

CD4$^+$ T cells

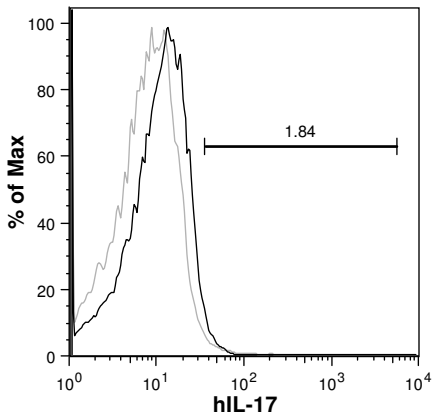

CD8$^+$ T cells